Sensitivity of a World Ocean GCM to Changes in Subsurface Mixing Parameterization

ANTHONY C. HIRST AND WENJU CAI

CSIRO Division of Atmospheric Research, Aspendale, Victoria, Australia

(Manuscript received 4 February 1993, in final form 17 September 1993)

ABSTRACT

The sensitivity of a coarse-resolution model of the World Ocean to parameterization of subgrid-scale mixing is examined. The model is based on the GFDL code. Results are presented from a series of model runs where the subsurface mixing parameterization is sequentially upgraded toward a more physical representation. The surface forcing is the same for all principal model runs and features a strong relaxation of surface temperature and salinity toward perpetual wintertime observed values. One model version is rerun with a full annual cycle of surface forcing and verifies that use of the perpetual winter surface relaxation introduces only minor biases in the essential characteristics of the solution.

Runs 1 and 2 feature the diffusivity tensor in the traditional horizontal/vertical orientation, and examines the effect of different vertical diffusivity profiles on the solution. Results are compared with those of previous studies. In both cases, the water mass properties (especially the salinity fields) are rather poor. In runs 3–5, a standard parameterization is introduced that allows for enhanced diffusion along the isopycnal surfaces. Each of these runs feature a different prescribed profile of isopycnal diffusivity, though with the same profile of vertical diffusivity as for run 2. Introduction of isopycnal mixing considerably improves the water mass structure, in particular by freshening and cooling water at intermediate depths toward realistic levels. However, the vertical stratification and density fields are little changed from run 2. Likewise, the current structure and meridional overturning are little changed. Thus isopycnal mixing has a major effect upon the temperature and salinity fields, but very minor effect on the ocean dynamics. Isopycnal mixing is found to modestly increase poleward oceanic heat transport in the midlatitudes via enhanced quasi-horizontal mixing of warm salty subtropical and cold fresh subpolar waters.

In run 6, the isopycnal diffusivity of run 4 is retained, but the vertical diffusivity is instead allowed to vary as the inverse of the local Brunt–Väisälä frequency. However, the resulting solution is little changed from that of run 4. Reasons for this small change are discussed. Also discussed are the impact of numerical problems associated with the use of realistically small vertical diffusivity, and problems inherent in deep water formation in coarse-resolution models.

1. Introduction

There is general agreement among oceanographers as to the importance of adequately representing isopycnal and diapycnal mixing processes in numerical ocean models. Rapid mixing of tracers by eddies in the real ocean is believed to occur primarily along neutral surfaces (i.e., surfaces of constant potential density, locally referenced; see McDougall 1987a). Mixing along these surfaces, which are generally not horizontal, is referred to as "isopycnal mixing." Mixing across the neutral surfaces, or "diapycnal mixing," proceeds much more slowly (e.g., Kraus 1990). In terms of Fickian diffusion, tracer diffusivities should be large along and small across the neutral surfaces. Instead, however, general circulation models (GCMs) of the large-scale ocean circulation have typically assumed large diffusivity in the horizontal and small diffusivity in the vertical (e.g., Bryan and Lewis 1979; Bryan 1987; Cox 1989). Such incorrect orientation of the mixing tensor could significantly affect the model solution, especially in regions where the neutral surfaces are steeply sloping.

Only very recently have attempts been made to include the correct mixing orientation in large-scale ocean models. One approach may seem to be to express the model in isopycnal coordinates as opposed to the traditional horizontal/vertical grid. However, this approach does not fully solve the problem, since McDougall (1987a) has shown that neutral surfaces often slope quite differently to isopycnal surfaces where the potential density is referenced to the surface. For models with a horizontal/vertical grid, Cox (1987a) introduced a scheme for mixing tensor rotation, based on the analysis of Redi (1982). This scheme uses potential density gradients referenced locally, and thus computes the orientation of the neutral surface correctly, in principle. The scheme received relatively little attention for some years; it is computationally fairly expensive, it requires retention of an artificial horizontal diffusivity

Corresponding author address: Dr. Anthony C. Hirst, CSIRO Division of Atmospheric Research, Private Bag No. 1, Mordialloc, Victoria 3196, Australia.

E-mail: ach@dar.csiro.au

for numerical stability, and it neglects some potentially significant effects of eddy mixing on isopycnal surfaces (Gent and McWilliams 1990). Nevertheless, the scheme does facilitate greatly enhanced mixing along the sloping neutral surfaces.

Cummins et al. (1990) implemented the Cox (1987a) isopycnal mixing scheme in their basin ocean model but reported only minor changes in tracer values, stratification, and meridional heat transport. England (1993) introduced the scheme into a World Ocean model and showed that it significantly contributed to freshening of the model's Antarctic Intermediate Water (AAIW). The isopycnal mixing scheme has recently been included in several World Ocean models (e.g., Dixon 1991, personal communication); however, sensitivity of the model solutions to parameters therein remains largely unexplored.

It is widely recognized that *diapycnal* mixing, though much slower than isopycnal mixing, is the mixing essential to the maintenance of the ocean's overturning circulation. Isopycnal mixing by definition cannot transport buoyancy, only diapycnal mixing can transport buoyancy downward to drive the deep circulation. Model experiments (e.g., Bryan 1987; Cummins 1991) have demonstrated the major effect that changes in the vertical (approximately diapycnal) diffusivity have on the thermocline structure and the strength of the meridional overturning circulation. Thus, realistic representation of this parameter is very important for the success of the model simulation. Below the wind mixed layer, most models either use a spatially fixed diffusivity (e.g., Cox 1989) or a diffusivity of fixed vertical structure (e.g., Bryan and Lewis 1979). The weakness of such schemes is that they do not respond to the potential influence of local factors on the diffusivity.

During the past decade, a body of evidence has developed that suggests that the diffusivity associated with *diapycnal* mixing in the ocean interior is roughly proportional to the inverse of the Brunt–Väisälä frequency (N) (e.g., Gargett 1984; Moum and Osborn 1986; Kraus 1990). If such were the case, then typical profiles of diapycnal diffusivity would differ greatly between the tropics and the polar or subpolar oceans, as a result of large differences in the profiles of static stability. Cummins et al. (1990) introduced an N^{-1} dependence of the diapycnal diffusivity into an ocean basin model and found moderate changes in the circulation and water mass properties. The effect of such a change in a global model, with its more complicated distribution of water masses, remains to be seen.

In the present study, we conduct a series of runs with a global ocean model to examine the effects of 1) varying the profile of vertical diffusivity, 2) introducing enhanced isopycnal mixing, 3) varying the profile of isopycnal diffusivity, and 4) introducing an N^{-1} dependence of the diapycnal diffusivity. In the first run, the model has no parameterization for isopycnal mixing and the vertical diffusivity is set to a uniform 1 $cm^2\ s^{-1}$. In the second run, depth dependence is introduced into the vertical diffusivity profile, with small values ($0.2\ cm^2\ s^{-1}$) in the upper ocean and larger values ($\sim 1\ cm^2\ s^{-1}$) at depth. In runs 3–5, enhanced isopycnal mixing is introduced via the Cox (1987a) scheme, with each run featuring a different prescribed profile for the isopycnal diffusivity. Finally, in run 6, enhanced isopycnal mixing is retained, and the diapycnal diffusivity is given an N^{-1} dependence. Wind stress and surface relaxation fields are identical for all the runs.

A primary goal of global ocean modeling is to provide the ocean component for a coupled ocean–sea ice–atmosphere model for the purpose of climate sensitivity experiments. Central to such an endeavor is the ability of the model to simulate the sea surface temperature (SST). However, the SST is a result of complex interactions between the ocean, sea ice, and atmosphere, and errors in the specification or simulation of these extraoceanic effects are likely to produce a poor SST simulation, regardless of the quality of the ocean model (e.g., Moore and Gordon 1994). Consequently, we concentrate here on the effect that changes in model physics have on the internal oceanic solution, given a surface forcing designed to keep the ocean surface temperature and salinity close to observed values. In particular, we shall examine the simulated stratification and water mass properties, because of the relatively detailed knowledge of such in the real ocean, and meridional heat transport, because of its climatic importance. Improvements in the simulation of such quantities may give us some confidence that the ocean model, when coupled to a superior atmosphere–sea ice model, would be able to give improved SST fields.

The paper is organized as follows. The model and individual runs are detailed in section 2. The surface forcing is discussed in section 3. The model integration procedure is detailed in section 4. Results of runs 1–6 are presented in section 5. The results of several auxiliary runs are presented in section 6. A discussion of problems associated with model deep water formation is given in section 7.

2. Model and runs

Apart from the changes to be made in the parameterization of scalar (i.e., temperature, salinity) mixing, the global ocean model used here is essentially the same as that used by Hirst and Godfrey (1993, hereafter HG). The model is based on the Bryan–Cox code (Cox 1984). The horizontal grid spacing is 1.5928° latitude by 2.8125° longitude. The model has 12 levels at depths shown in Table 1. The horizontal and vertical viscosities are spatially constant, with the values 1.2×10^9 $cm^2\ s^{-1}$ and 20 $cm^2\ s^{-1}$. Details of the diffusivities, which are varied between the runs, are given later in the section. Weaver and Sarachik (1990) note that the

TABLE 1. Vertical spacing used in the experiments (depths in meters).

Model level	Depth of grid point	Depth of grid box bottom	Thickness of grid box
1	12.5	25	25
2	37.5	50	25
3	70	90	40
4	125	160	70
5	215	270	110
6	370	470	200
7	635	800	330
8	1025	1250	470
9	1575	1900	650
10	2350	2800	900
11	3250	3700	900
12	4150	4600	900

present vertical resolution (12 levels) may cause numerical artifacts that disappear with higher resolution. We verify the validity of the present solutions by repeating one of the experiments with a 21-level model (as detailed in the Appendix).

The present runs use a bottom topography slightly altered from that of HG. First, the Indonesian passage is widened and simplified, and the sill depth increased to 1250 m. We shall test whether the excessive throughflow found by HG for such a channel is linked to their prescription of a large uniform vertical diffusivity. Second, the Denmark Strait sill depth has been increased from 270 m to 800 m. The former depth was an artifact of HG's topography interpolation; the observed sill depth is about 600 m (which lies midway between two grid-box lower surfaces). The resulting increase in sill overflow leads to substantially colder (i.e., more realistic) North Atlantic Deep Water (NADW). The model geometry is shown in Fig. 1. Nonzero barotropic circulation is permitted about each of the eight islands.

Outflow of Red Sea Water is parameterized via a slow relaxation of temperature and salinity at the two coastal grid points in the Gulf of Aden at 270–470 m depth toward values observed for outflow water (i.e., 23.0°C and 39.7 psu; Cember 1989). The relaxation e-folding decay time of 680 days corresponds to an addition of 0.36 Sv (Sv $\equiv 10^6$ m^3 s^{-1}) of Red Sea Water (Cember 1989) averaged over the combined volume of these grid boxes. Outflow of Mediterranean Sea water is parameterized by mixing Mediterranean and Atlantic water laterally between opposing grid boxes across the unresolved Strait of Gibraltar, over the depth range 270–1250 m. Here, mixing time scales were calculated assuming a 0.8 Sv exchange (Bryden and Kinder 1991) averaged over the combined volume of the indicated grid boxes.

Details of the principal model runs are summarized in Table 2. As discussed in section 1, the first two runs are without isopycnal mixing. Run 1 features the uniform and rather large vertical diffusivity (A_{TV}) used by HG. An alternative profile of A_{TV} is prescribed in run 2 and is shown in Fig. 2a. The profile features a linear increase in A_{TV} with depth, and is a simplification of that calculated by Kraus (1990, his Fig. 2) from the observed (Levitus 1982) density distribution and an assumed N^{-1} dependence of the diffusivity. A lower limit on A_{TV} of 0.2 cm^2 s^{-1} is set for numerical reasons, although a smaller value ($\sim$0.1 cm^2 s^{-1}) may be justified in the upper ocean, at least in the tropics/subtropics (e.g., Moum and Osbourne 1986). The present profile differs significantly from that adopted by Bryan and Lewis (1979), with smaller diffusivity in the upper

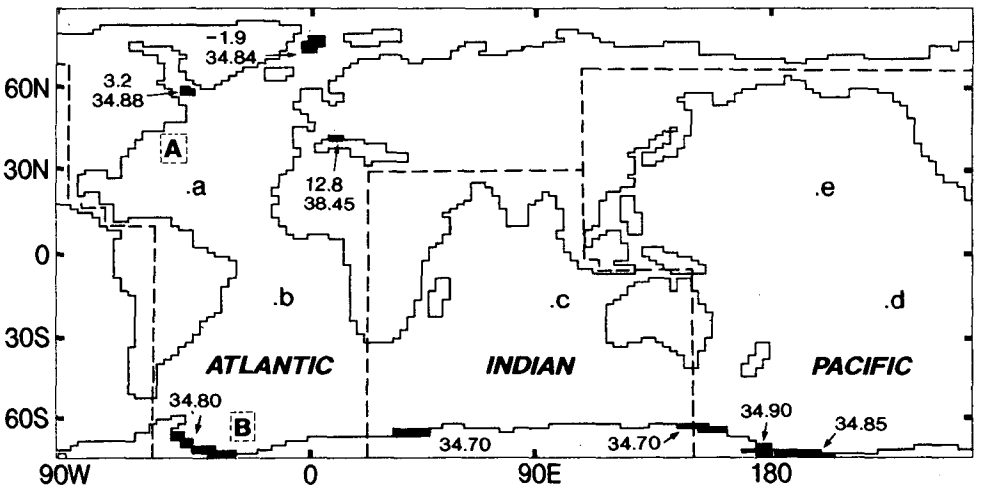

FIG. 1. Geometry of the model ocean. Heavy dashed lines indicate boundaries of the ocean sectors used for zonal-average T–S plots. Thin dashed lines indicate boundaries of areas A and B, referred to in Table 3. Black fill indicates areas in which the surface relaxation fields for T and/or S have been corrected to the given values (units are °C and psu). Also shown are points (a) to (e), referred to in the text.

and deep ocean, and larger diffusivity at intermediate depths.

Runs 3–5 feature enhanced isopycnal mixing as per the scheme distributed by Cox (1987b). Under this scheme, the mixing orientation is rotated according to the tensor

$$K = A_{TI}\begin{pmatrix} 1+\epsilon_H & 0 & \rho_x/s \\ 0 & 1+\epsilon_H & \rho_y/s \\ \rho_x/s & \rho_y/s & \epsilon_V + (\rho_x^2\,\rho_y^2)/s^2 \end{pmatrix}. \quad (1)$$

The tensor (1) is simplified via scale analysis from the complete tensor given by Redi (1982). Here A_{TI} is the isopycnal diffusivity and (ρ_x, ρ_y, ρ_z) are the gradients of potential density computed using coefficients defined for the local salinity, temperature, and pressure. Also, $\epsilon_H = A_{TH}/A_{TI}$, where A_{TH} ($= 0.7 \times 10^7$ cm^2 s^{-1}) is the unphysical horizontal diffusivity retained for numerical reasons, and $\epsilon_V = A_{TV}/A_{TI}$, where A_{TV} is the physically based diapycnal diffusivity [note that this acts only in the vertical under the simplified tensor (1), and will henceforth be referred to as "vertical diffusivity"].

The parameter $s = \max[-\rho_z, (\rho_x^2 + \rho_y^2)^{1/2}/\tan\alpha]$ and replaces the $-\rho_z$ of the complete tensor. Thereby, the slope of the mixing surface cannot exceed a prescribed α, though the horizontal direction of that surface's gradient remains the same as for the neutral surface at that point. This slope limitation is necessary in order to avoid numerical instability (Cox 1987b). In all present runs involving isopycnal mixing, we set the maximum slope ($\tan\alpha$) to 1/100. In the present solutions, application of this constraint is mostly restricted to the vicinity of convective mixed layers, in which the true neutral surfaces are essentially vertical. Such mixed layers make up only a few percent of the total ocean volume, though they are important in water mass formation. To test the sensitivity of the solution to the prescribed maximum slope, we repeated one run (run 4) with the maximum slope set to the smaller 1/250 and found only minor changes. The effect of the above constraint on convective mixed layers is further discussed in the Appendix.

Each of runs 3–5 feature a different prescribed profile of isopycnal diffusivity (A_{TI}), shown in Fig. 2b. In run 3, A_{TI} is set to be a uniform 1×10^7 cm^2 s^{-1} (after Cummins et al. 1990). In run 4, A_{TI} decays with an e-folding depth of 500 m from a large surface value of 5×10^7 cm^2 s^{-1} toward a deep value of 1×10^7 cm^2 s^{-1}

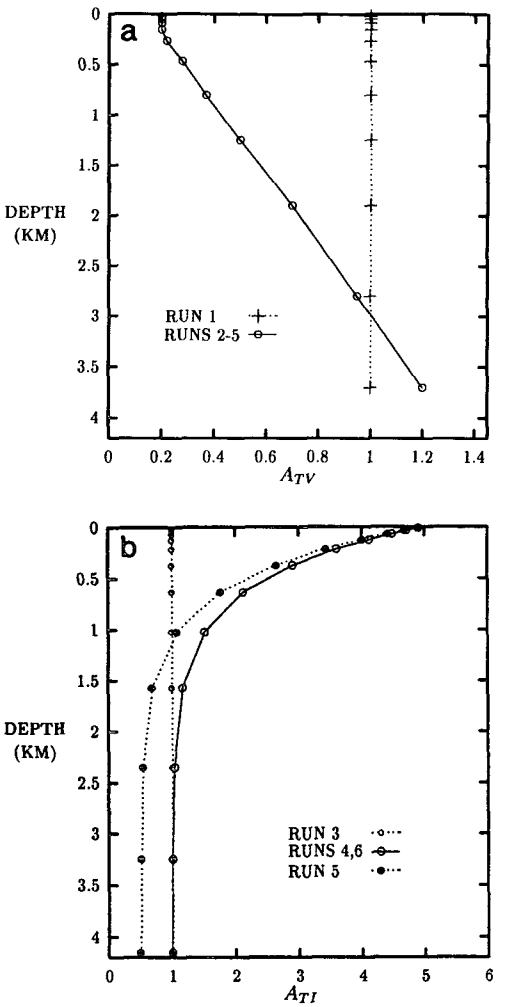

FIG. 2. Prescribed profiles of (a) vertical diffusivity A_{TV}, and (b) isopycnal diffusivity A_{TI}, for the indicated runs: A_{TV} has units cm^2 s^{-1}; A_{TI} has units 10^7 cm^2 s^{-1}.

TABLE 2. Summary of mixing schemes in principal model runs. Orientation of mixing tensor is either "H/V" (horizontal/vertical) or "I/D + H" (isopycnal/diapycnal plus additional horizontal diffusivity). Columns "A_{TV} (0)" and "A_{TV} (z_b)" list upper-ocean and bottom vertical diffusivity, respectively. Columns "A_{TI} (0)" and "A_{TI} (z_b)" list surface and bottom isopycnal diffusivity, respectively (diffusivities have units cm^2 s^{-1}).

Run	Orientation	A_{TV} (0)	A_{TV} (z_b)	A_{TI} (0)	A_{TI} (z_b)
1	H/V	1.0	1.0	—	—
2	H/V	0.2	1.2	—	—
3	I/D + H	0.2	1.2	1×10^7	1×10^7
4	I/D + H	0.2	1.2	5×10^7	1×10^7
5	I/D + H	0.2	1.2	5×10^7	0.5×10^7
6	I/D + H	α_0/N (0.2 min)	α_0/N (0.2 min)	5×10^7	1×10^7

[after Dixon (1991, personal communication) and England (1992, 1993)]. Since A_{TI} remains little changed below about 1500 m, a comparison of runs 3 and 4 primarily indicates the effect of much enhanced upper-ocean isopycnal diffusion. The A_{TI} profile for run 5 retains the large surface value but decays toward the deep value of 0.5×10^7 cm^2 s^{-1}. Comparison with run 4 indicates the effect of reduced subsurface, and especially deep ocean, isopycnal diffusion. The vertical diffusivity in runs 3–5 is as in run 2 (Fig. 2a).

Run 6 is identical to run 4 except that vertical diffusivity is made proportional to N^{-1},

$$A_{TV} = \frac{a_0}{N} = a_0 \Big/ \left(-\frac{g}{\rho_0} \rho_z \right)^{1/2}, \qquad (2)$$

where ρ_0 is a reference density, and $a_0 = 1 \times 10^{-3}$ cm^2 s^{-2} (after Gargett 1984). A lower limit of 0.2 cm^2 s^{-1} is again imposed on A_{TV}.

Convective mixing is simulated by applying an enhanced vertical diffusivity, of 10^6 cm^2 s^{-1}, in regions of static instability. This value is larger than the 10^4 cm^2 s^{-1} often prescribed (e.g., Cox 1987c) and is chosen to ensure a clear separation between the time scales of quasi-vertical adjustment via direct convection and via mixing along steeply sloping isopycnals. However, trial experiments indicated little change in the model solution for values in the range 10^4 cm^2 s^{-1} to 10^7 cm^2 s^{-1}. No parameterization is included to deepen the surface mixed layer by wind forced mixing. Convection resulting from static instability is thus the only mechanism for mixed layer deepening.

In sections 6a and 6b, we repeat runs 2, 4, and 6 under some different physical assumptions in order to examine the robustness of the present results. The potential impact of the unphysical horizontal diffusivity A_{TH} on the solution is discussed in section 6a, where results from runs "2h," "4h," and "6h" are presented. These runs are identical to runs 2, 4, and 6 except that A_{TH} is *doubled*. The potential impact of wind-forced mixing on the solution is discussed in section 6b, where results from runs "2ml," "4ml," and "6ml" are presented. These runs are identical to runs 2, 4, and 6 except that a weak enhancement of near-surface A_{TV} is prescribed. The size of the enhancement is chosen so as to make the spatially averaged near-surface density profile concur with observations.

3. Surface forcing

In this study, top-level temperature and salinity are relaxed back to perpetual *wintertime* ocean surface climatology. The wintertime values are adopted based on the assumption that water mass characteristics for most of the ocean volume are primarily set during late winter convection. Thin summer mixed layers of the middle to high latitudes typically sit atop a thick layer of denser water comprising the remnant of the previous winter mixed layer (e.g., Martin 1985). In the absence of strong downward Ekman pumping or strong wind-forced mixing, we expect this winter water layer to be little affected by the ephemeral light summer water above it, and so act as the source water for eventual subduction and water mass formation.

Ocean model studies often employ time-invariant (rather than annual cycle) upper-boundary conditions for reasons of economy of output and analysis, and to fully exploit the techniques of Bryan (1984) for accelerated equilibration of the model solution. Commonly, *annual mean* ocean surface climatology is used (e.g., Toggweiler et al. 1989a; HG), although this is believed to lead to problems with water mass properties. For example, deep water in such simulations tends to be too fresh, which is believed to partly result from the spurious impact of fresh summer meltwater layers on the forcing salinities in the deep water formation regions. To check the extent to which the present use of perpetual winter climatology affects ocean model behavior, run 5 is repeated using a full annual cycle of surface forcing. Resulting differences in the solutions are minor, and are discussed in section 6c.

In contrast to the perpetual winter boundary conditions on temperature and salinity, we subject the ocean to the *annual mean* Hellerman and Rosenstein (1983) wind stress. Winter wind stress is not used because such stress applied perpetually is found to produce spurious strengthening of the ACC and major gyres, and thereby substantially increased poleward heat transport. Such strengthening, which is in excess of the annual range, occurs because the time scale of oceanic adjustment to changes in wind stress is the transit time of low-order Rossby waves across the basin, which is of order years. The annual cycle of wind stress has a frequency too high to effect a complete adjustment of the gyres.

The winter fields of temperature and salinity to be used in the relaxation are, over most of the ocean, derived from the Levitus (1982) climatology interpolated horizontally and vertically to the model's top-level grid. The Levitus temperature field for March and salinity field for February/March/April are used to the north of 5°N (approximately the "thermal equator"), while those for September and August/September/October are used south of this line. The fields are smoothed over several grid points across the demarcation.

Unfortunately, formation of realistic water masses is in some cases impossible under near-surface Levitus climatology. An inspection of the original Levitus values for the 10 m depth (which dominates in the interpolation to 12.5 m depth) reveals serious inconsistencies with observations in many important water formation regions.[1] In the Labrador Sea, Levitus values

[1] There are also some surprising inconsistencies between the surface (0 m) and 10 m values of Levitus. For example, peak Norwegian/Iceland Sea densities are 0.02 kg m^{-3} *higher* for the surface values

give a peak density of $\sigma_t = 27.73$ kg m^{-3}, instead of the observed 27.78 kg m^{-3} (Clarke 1985). In the Norwegian/Iceland/Greenland Sea, Levitus values give a peak density of 27.95 kg m^{-3}, whereas observations indicate two extensive regions of surface density greater than 28.0 kg m^{-3} (Swift et al. 1980; Rudels et al. 1989; Clarke et al. 1990). Dense waters from the above regions are central to the formation of NADW (e.g., Swift et al. 1980). Such problems with the Levitus data are compounded upon interpolation to the coarse model grid, since model grid points rarely coincide with the position of densest water as given by Levitus.

To give the ocean model the chance to form realistic water masses, we alter the surface relaxation fields in key regions to reflect observed or inferred late winter surface properties (see also England 1922). The modifications are summarized in Fig. 1. In the North Atlantic region, relaxation temperatures and salinities in the Gulf of Lyons and central Labrador Seas are altered to late winter surface values observed to participate in deep convection. The values assigned to the central Labrador Sea are intermediate between those inferred for the 1960s and fresher, cooler values observed in the late 1970s (Clarke 1985). In the northern Greenland Sea, values are inferred by extrapolation to freezing point of the $\sigma_t = 28.06$ water observed in the convective column discovered by Rudels et al. (1989) (the convection appears associated with transient sea ice formation).

Near Antarctica, salinity corrections are applied to the southern and western Ross and Weddell Seas, with values based on observed shelf water salinities. The high salinity shelf water is believed important in the formation of Antarctic Bottom Water (ABW) (Carmack 1986; Grumbone 1991). Three rules are followed for the application of the Antarctic corrections. Firstly, correction is generally restricted to points within two grid spacings of the coast. Secondly, correction is restricted to points where the seafloor is at depth 800 m or less. Thirdly, correction is not permitted at points where the depth of the seafloor at a neighboring point is greater than 1900 m. These rules assume the importance of near-coastal salt exclusion (Grumbone 1991) and require that the resulting high salinity shelf water cannot reach the deep ocean without undergoing mixing and downslope flow, in accordance with observations (Killworth 1983; Carmack 1986). Highest salinities produced on the model Ross and Weddell shelves are typically 34.90 psu and 34.78 psu, respectively, which are fairly realistic. We also include relatively weak salinity corrections at some coastal points along the Adelie and Enderbury Coasts, to allow for downslope flow there into the deep ocean, in accordance with observations (e.g., Killworth 1983).

than for the 10 m values. Run 5 was repeated using the Levitus surface fields plus the corrections noted in the text, but changes in the large-scale water masses were minor.

Note that the model's surface water does not achieve the peak observed densities in any of the above regions, because of mixing/advection involving neighboring less dense water, and the finite time scale of the relaxation. For example, densities in the model north Greenland Sea typically peak at about $\sigma_t = 28.02$ kg m^{-3}.

The present study uses a very short *e*-folding time scale of 4 days for the surface relaxation. This contrasts with commonly used time scales based on a Haney coefficient of about 35 W m^{-2} °C, which corresponds here to an *e*-folding time of 33 days. Such a long *e*-folding time is not appropriate for studies involving examination of model water masses, since it leads *intrinsically* to large errors in the surface water properties. For example, a modest surface heat loss of 70 W m^{-2} would require that the model ocean temperature depart by +2°C from the observed climatology. Some of the runs presented here were repeated using an *e*-folding time of 40 days, and displayed a marked degradation in water mass structure. Alternative schemes (e.g., Han 1984; HG; Moore and Reason 1993) are not applicable here due to lack of atmospheric and sea ice data in the crucial polar regions. Again, our philosophy here is to (approximately) set the upper-surface properties and examine the internal model response.

To further test the sensitivity of the solutions to the *e*-folding time scale for surface relaxation, several of the runs were repeated with this time scale set at 10 days. Changes in the water masses were fairly minor, and all conclusions herein remained valid.

4. Experimental procedure

All of runs 1–6 were initialized using a common restart file. This restart file was obtained after an extensive preliminary run, starting from HG's "full throughflow" solution. During this preliminary run, the several model alterations noted in section 2 and the perpetual winter forcing were introduced.

All runs were continued until satisfactorily equilibrated. Since it is impossible to integrate to a completely equilibrated solution in finite time, we define the following convergence criterion: the solution is considered converged if rates of change of the global-mean temperature and salinity at each of levels 1–10 are less than 5×10^{-3} °C and 1×10^{-3} psu per century, and at levels 11 and 12 are half that amount. Acceleration techniques of Bryan (1984) were used to speed convergence of the model solution. The barotropic streamfunction and baroclinic velocity equations were integrated with a time step of 20 minutes. The time step for the scalars [temperature (T) and salinity (S)] varied with depth, being set at 1 day for levels 1–5 and steadily increased at lower levels to 8 days at level 12.

The solutions took between 450/3600 years and 700/5600 years of integration to converge. To test for the effect of residual drift, several runs (1, 4, and 6)

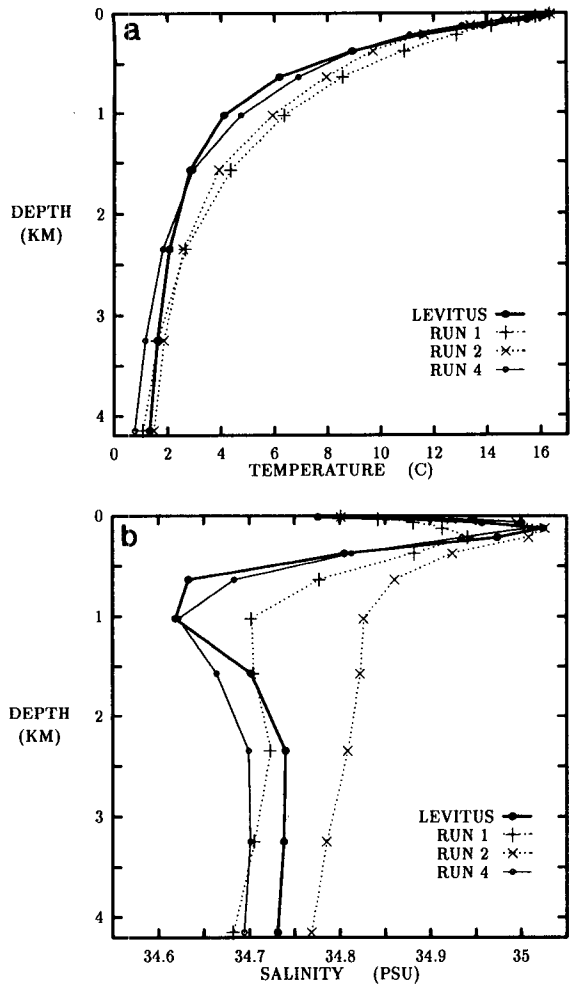

FIG. 3. Globally averaged profiles of (a) temperature and (b) salinity for runs 1, 2, and 4. Profiles derived from Levitus (1982) data interpolated to the model grid are also shown (solid line). (Units are °C and psu, depth is in km.)

were extended for a further 100/800 years. In each case, the drifts dropped to about half the criterion values, with negligible change in solution.

Auxiliary runs 2h, 4h, 6h, 2ml, 4ml, and 6ml were restarted from the respective final quasi-equilibrium solutions of runs 2, 4, and 6. These auxiliary runs typically took of the order 350/2800 years to converge.

The above acceleration techniques were found to produce minor biases when applied to the case with annual-cycle forcing. The time stepping used in this case is discussed in section 6c.

5. Results of principal runs

a. Change in vertical diffusivity profile

The effect of changing the vertical profile of A_{TV} is examined via a comparison of the solutions for runs 1 and 2. Comparison here will be brief, since many changes mirror those expected from previous studies (e.g., Bryan 1987; Cummins 1991).

There are substantial differences in the water mass properties between runs 1 and 2. Figure 3 shows profiles of globally averaged temperature and salinity for both solutions, together with winter values interpolated from the Levitus (1982) data. Clearly apparent in Fig. 3a is the excessively deep and diffuse thermocline in the case of run 1 (large uniform A_{TV}). The thermocline structure is only slightly improved in run 2. However, Fig. 3b shows that run 2 yields much saltier deep water than run 1. The increase in salinity is greatest in the Southern and Pacific Oceans and appears associated with reduced downward mixing of fresh surface water in the ocean surrounding Antarctica. However, the water mass simulation is poor in both cases (e.g., the marked salinity

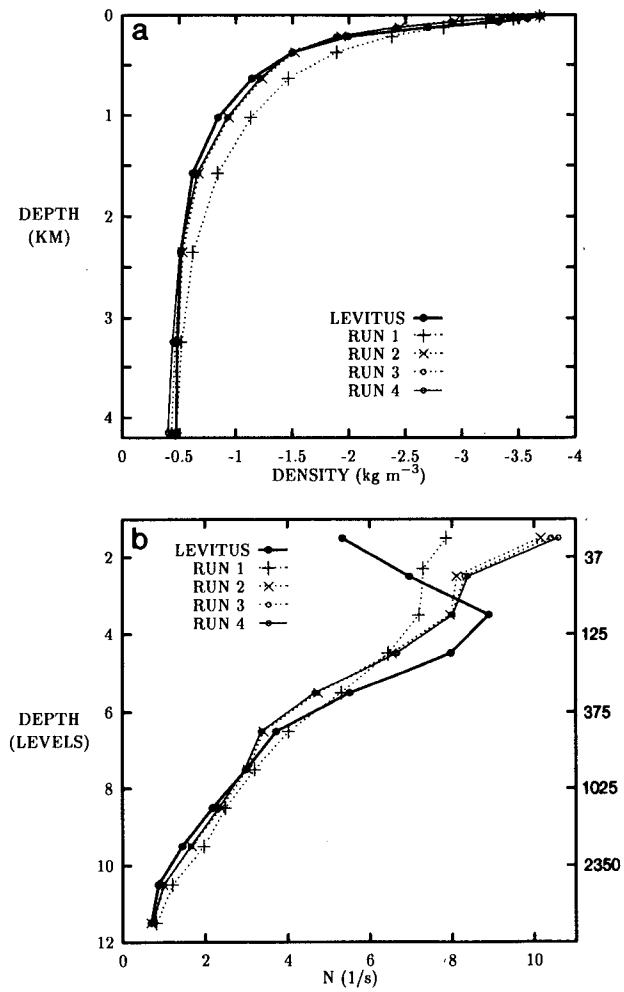

FIG. 4. Profiles of (a) in situ density ($\sigma_{s,t,p} - \sigma_{35,0,p}$) and (b) Brunt–Väisälä frequency (N), averaged between 45°N and 45°S, for runs 1–4 and for Levitus T and S (after interpolation to model grid). (Units are kg m^{-3} and s^{-1}.)

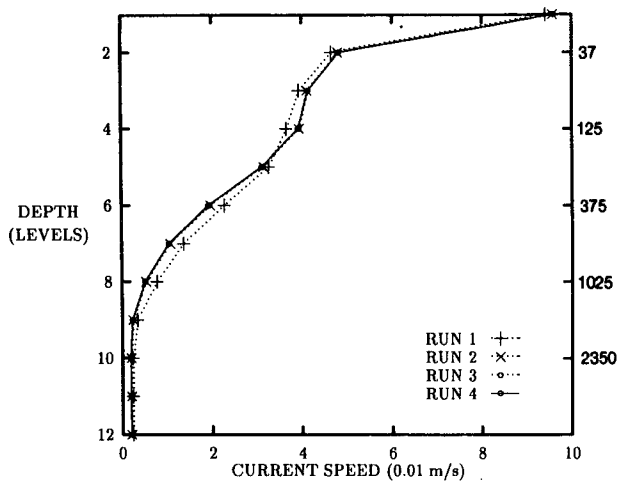

FIG. 5. Profile of current speed averaged between 45°N and 45°S, for runs 1–4. (Units are cm s^{-1}.)

minimum at about 1000 m depth is almost completely missing), and detailed comparison is unwarranted.

Figure 4a shows profiles of density ($\sigma_{S,T,p} - \sigma_{35,0,p}$) for runs 1–4 and for observations, averaged between 45°N and 45°S. The use of reduced A_{TV} in run 2 yields a much more realistic density profile between 200 m and 3000 m depth. In run 2, both T and S are unrealistically high at such depth (Fig. 3), but the resulting effects on density nearly balance.

The vertical stratification is indicated in Fig. 4b, which shows profiles of the Brunt–Väisälä frequency (N), again averaged between 45°N and 45°S. Run 2 yields stronger stratification in the upper 215 m and weaker stratification at greater depth than run 1. The deep ocean changes are broadly consistent with the rather surprising result of Bryan (1987) and Cummins (1991) that decreased vertical diffusivity (as in run 2) actually leads to decreased deep ocean stratification, in their basin models. Deficiencies in the upper 200 m associated with neglect of surface mixing processes are discussed in section 6b.

The change in stratification between runs 1 and 2 has an impact on model currents. Figure 5 compares the current speeds averaged between 45°N and 45°S at each model level. Run 2 exhibits larger current speeds in the top 160 m but smaller currents at greater depth. This pattern presumably results from the dominance of wind forcing over thermal forcing of currents in that latitude band. Wind stress is unchanged between the runs, and so the depth-integrated Sverdrup circulation would remain unchanged. However, the stratification in run 2 is more concentrated near the surface, and so the wind-driven currents are more closely confined to the surface. To achieve the same depth-integrated transport, the shallower currents must flow faster.

The strength of the Antarctic Circumpolar Current (ACC) in each of the model runs is listed in Table 3. A considerable weakening of this current occurs from run 1 to run 2. This indicates that the ACC has a substantial thermal component, at least in run 1. The current weakens in response to the reduced cross-current density gradients at depth, resulting from the weakened stratification to the north of the current.

Also shown in Table 3 is the net transport through the Indonesian passage for each model run. We see that the transport declines to near the value expected from Sverdrup theory (16 ± 4 Sv; Godfrey 1989) when the diffusivity is reduced. This suggests that the large values attained by HG and in the present run 1 result from an interaction between the passage topography

TABLE 3. List of attributes from the solution of each model run. Shown are net Indonesian Throughflow (IT), strength of Antarctic Circumpolar Current as given by the Drake Passage Throughflow (ACC), strength of NADW formation as given by the maximum in the Atlantic overturning streamfunction ($NADW_{max}$), outflow of NADW across the equator again as indicated by the Atlantic overturning streamfunction ($NADW_{eq}$), T and S at 3250 m depth averaged over northwest Atlantic area A (T_{NA}, S_{NA}) and over Weddell Sea area B (T_{WS}, S_{WS}) (areas indicated on Fig. 1). Run 5s values are final-year means. Transports have units of Sv, temperatures are in °C, and salinities are in psu.

Run	IT	ACC	$NADW_{max}$	$NADW_{eq}$	T_{NA}	S_{NA}	T_{WS}	S_{WS}
1	23.3	183	31.0	21.3	3.3	34.91	−0.9	34.60
2	17.4	147	22.7	16.2	3.0	34.94	−0.5	34.67
3	17.6	153	22.9	16.1	3.0	34.94	−0.7	34.66
4	17.7	156	22.7	16.1	2.9	34.93	−0.9	34.66
5	17.7	155	22.7	16.2	2.9	34.93	−0.8	34.66
6	17.5	150	22.1	15.8	2.9	34.93	−0.9	34.66
2h	18.6	133	19.3	13.2	3.4	34.98	−0.4	34.64
4h	18.4	138	19.0	13.0	3.1	34.95	−0.8	34.62
6h	18.1	134	18.4	12.6	3.1	34.95	−0.9	34.62
2ml	17.5	148	22.6	16.4	3.1	34.94	−0.5	34.66
4ml	18.0	159	22.4	16.1	2.9	34.93	−1.0	34.64
6ml	17.6	153	21.7	15.7	2.9	34.93	−1.1	34.64
5s	17.9	157	22.3	15.5	3.4	34.93	−0.7	34.60
Observed	—	—	—	—	2.4	34.94	−0.5	34.67

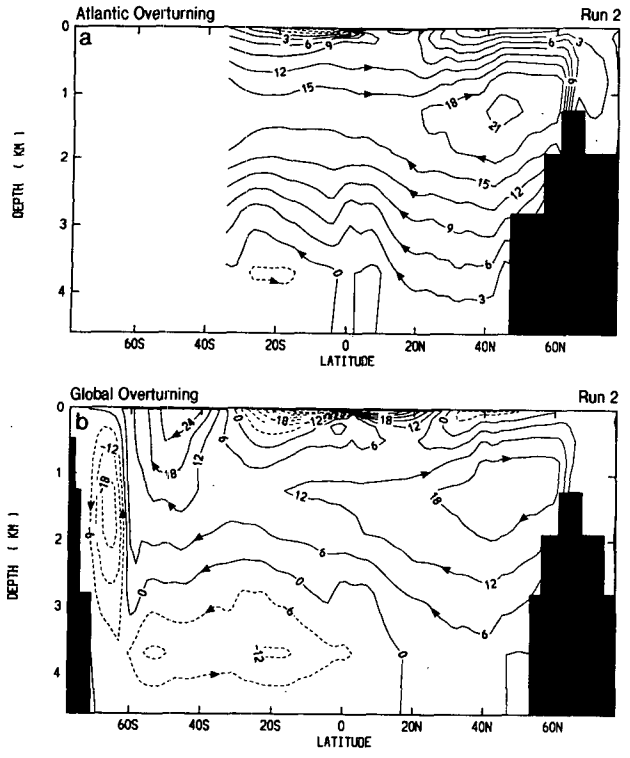

FIG. 6. Meridional overturning streamfunction for run 2 for (a) the Atlantic Ocean and (b) the global ocean. (Units are in Sv.)

and the unrealistically deep thermocline in those runs. In any case, the overall current structure of the South Indian Ocean in both runs 1 and 2 remains essentially as discussed in HG for their "full throughflow" case.

Meridional overturning streamfunctions for the Atlantic and the global ocean are shown in Fig. 6 for run 2. Apparent is a strong Atlantic "conveyor belt," with the southward NADW flow flushing to the bottom of the North Atlantic. This situation differs from many other modeling studies (e.g., Toggweiler et al. 1989a; England 1993; HG) where annual mean or uncorrected seasonal forcings were applied. In those studies, the "conveyer belt" pattern does not extend to the North Atlantic floor, and weak northward motion is evident there. In the present model, the deep penetration of NADW helps ensure that the influence of AABW in the model's deep North Atlantic remains realistically small. Similarly, the volume of NADW outflow is large compared to that typical of other modeling studies, but is close to recent estimates based on anthropogenic tracer observations (Molinari et al. 1992).

The patterns of overturning in runs 1 and 2 are qualitatively similar. The overturning is generally stronger in run 1 than run 2. The changes in the Atlantic circulation (see Table 3) are of the same order as expected from the 1/3 power law of Bryan (1987), if the diffusivity at 1250 m depth is taken to be representative.

Model meridional heat transports for (a) the globe, (b) the Atlantic, and (c) the Indian and Pacific Oceans are shown in Fig. 7. On comparing the results for runs 1 and 2, we see a substantial decline in heat transport associated with the reduction in upper ocean A_{TV}. Such a decline is expected based on previous studies (e.g., Bryan and Lewis 1979; Bryan 1987; Cummins et al. 1990), where discussions of its underlying causes may be found. In the present model, the extent of the decline varies between the ocean basins. The Atlantic trans-

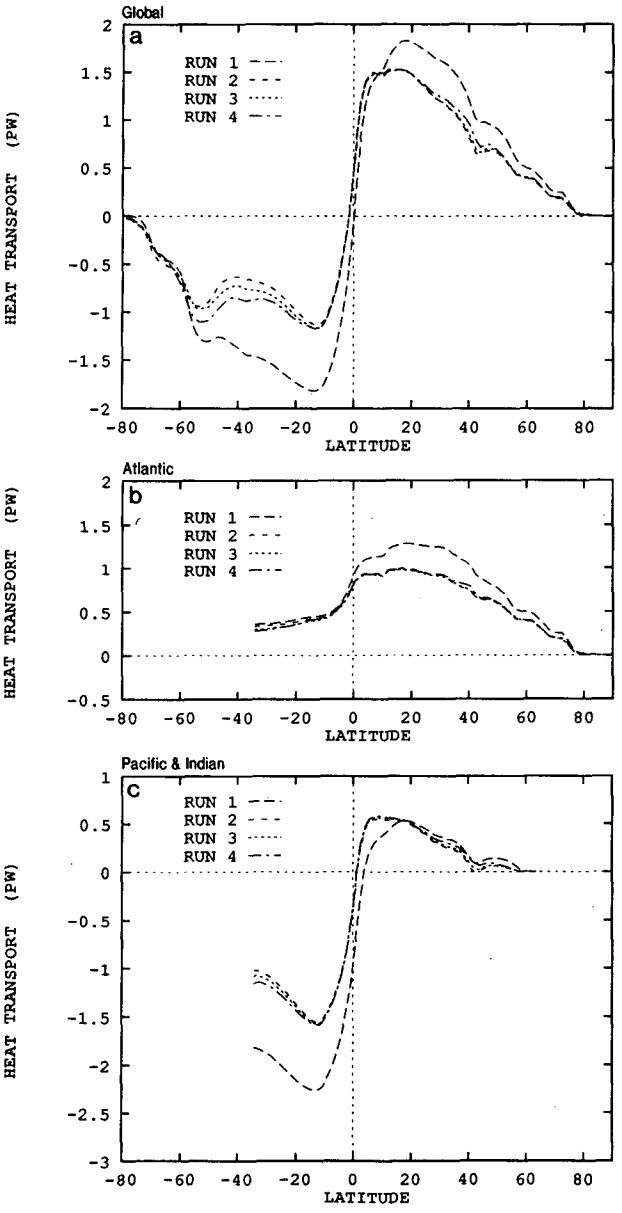

FIG. 7. Meridional heat transport (positive northward) for (a) the global ocean, (b) the Atlantic Ocean, and (c) the Indian and Pacific Oceans, for runs 1–4. Units are in PW. Values are derived by southward integration of the surface heat flux implicit in the temperature relaxation (averaged over the last 1000 steps of the model run).

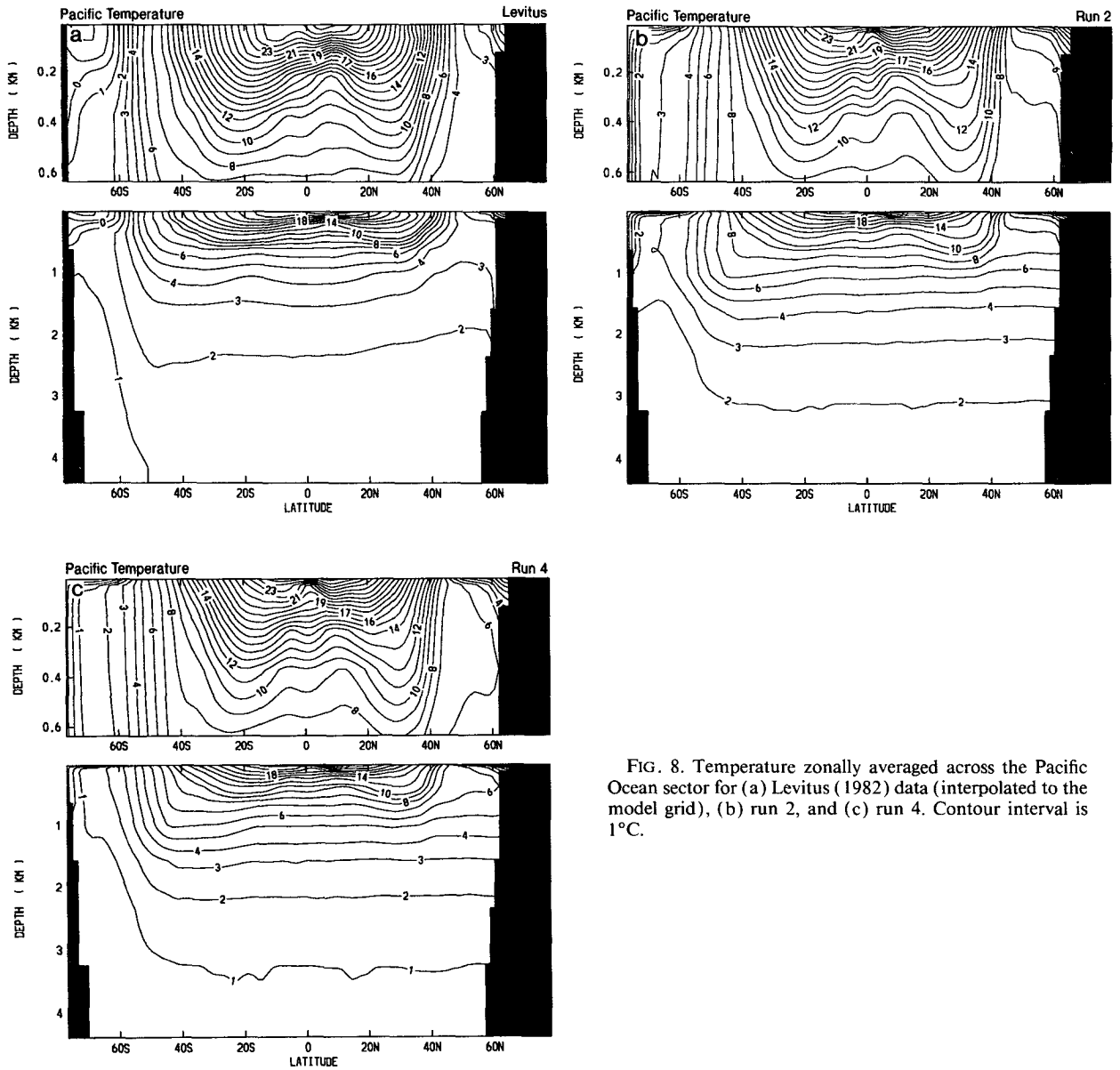

FIG. 8. Temperature zonally averaged across the Pacific Ocean sector for (a) Levitus (1982) data (interpolated to the model grid), (b) run 2, and (c) run 4. Contour interval is 1°C.

ports at 25°–30°N, of 1.26 PW for run 1 and 0.93 PW for run 2, are both satisfactorally close to the 1.0–1.25 PW annual mean estimated from observations via several methods (e.g., Molinari et al. 1990).

We finally note the effect of reduced A_{TV} on the depth and extent of surface convective mixing. This mixing provides the primary means by which heat transported horizontally at depth is released to the atmosphere (e.g., HG). As in HG, convection in run 1 tends to penetrate to excessive depth. Run 2 features less extensive convection, and the depth of penetration is generally less (by typically 25%–50%), thus it is more realistic. The shoaling of convection is to be expected as a result of the stronger upper-ocean stratification in run 2. However, the overall patterns of convection in runs 1 and 2 are qualitatively similar.

b. *Introduction of isopycnal mixing*

We begin with a more detailed examination of the water mass properties for run 2 (no isopycnal mixing). Figures 8–10 show zonally averaged temperature and salinity fields for the Pacific sector (as defined in Fig. 1) and salinity fields for the Atlantic sector, respectively. In each figure, panels (a) and (b) show the field derived from Levitus (1982) data and that for run 2, respectively. The thermal structure of the Pacific appears qualitatively realistic in run 2 (Fig. 8b), though temperatures are about 2°–3°C too high at intermediate

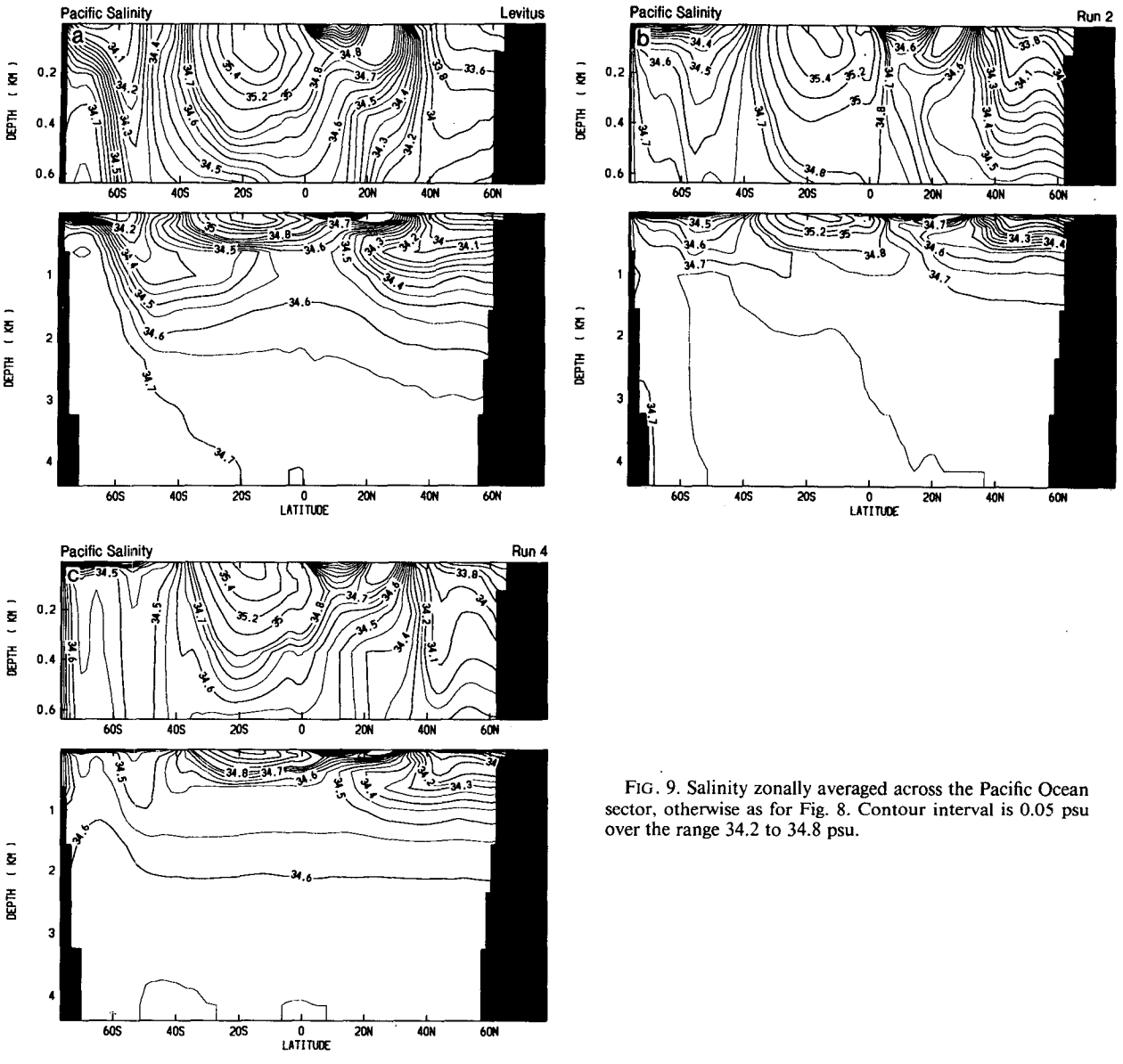

FIG. 9. Salinity zonally averaged across the Pacific Ocean sector, otherwise as for Fig. 8. Contour interval is 0.05 psu over the range 34.2 to 34.8 psu.

depth. The Pacific salinity structure (Fig. 9b) is relatively poor. In particular, the northward penetration of fresh AAIW is extremely weak. The tongue of fresh North Pacific Intermediate Water is also too weak. The deep water is excessively saline. The salinity structure of the Indian Ocean (not shown) is similarly poor. The Atlantic salinity structure (Fig. 10b) does bear qualitative resemblance to that of Levitus (Fig. 10a). Note the fairly realistic salinity and distribution of NADW and the realistically weak incursion of fresher AABW beneath the NADW. Some northward penetration of fresh AAIW is evident above the NADW; however, the intermediate salinity minimum is again too weak. Toggweiler et al. (1989a,b) found that the spread of AAIW was poor in a model fairly similar to that used in run 2.

The above discrepancies are further illustrated in Fig. 11, which shows T–S curves for the points (**a**)–(**e**) located as shown in Fig. 1, one in each of the five major ocean basins. Clearly evident in the curves for run 2 are the weakness or absence of the observed intermediate-depth salinity minimum at each point, and the excessive deep salinity of the Indian and Pacific Oceans. There are also substantial discrepancies in the water properties at lower thermocline depth ($T > 8$°C), but these show no systematic pattern.

The introduction of isopycnal mixing has a major effect on the model T and S fields, even for the relatively

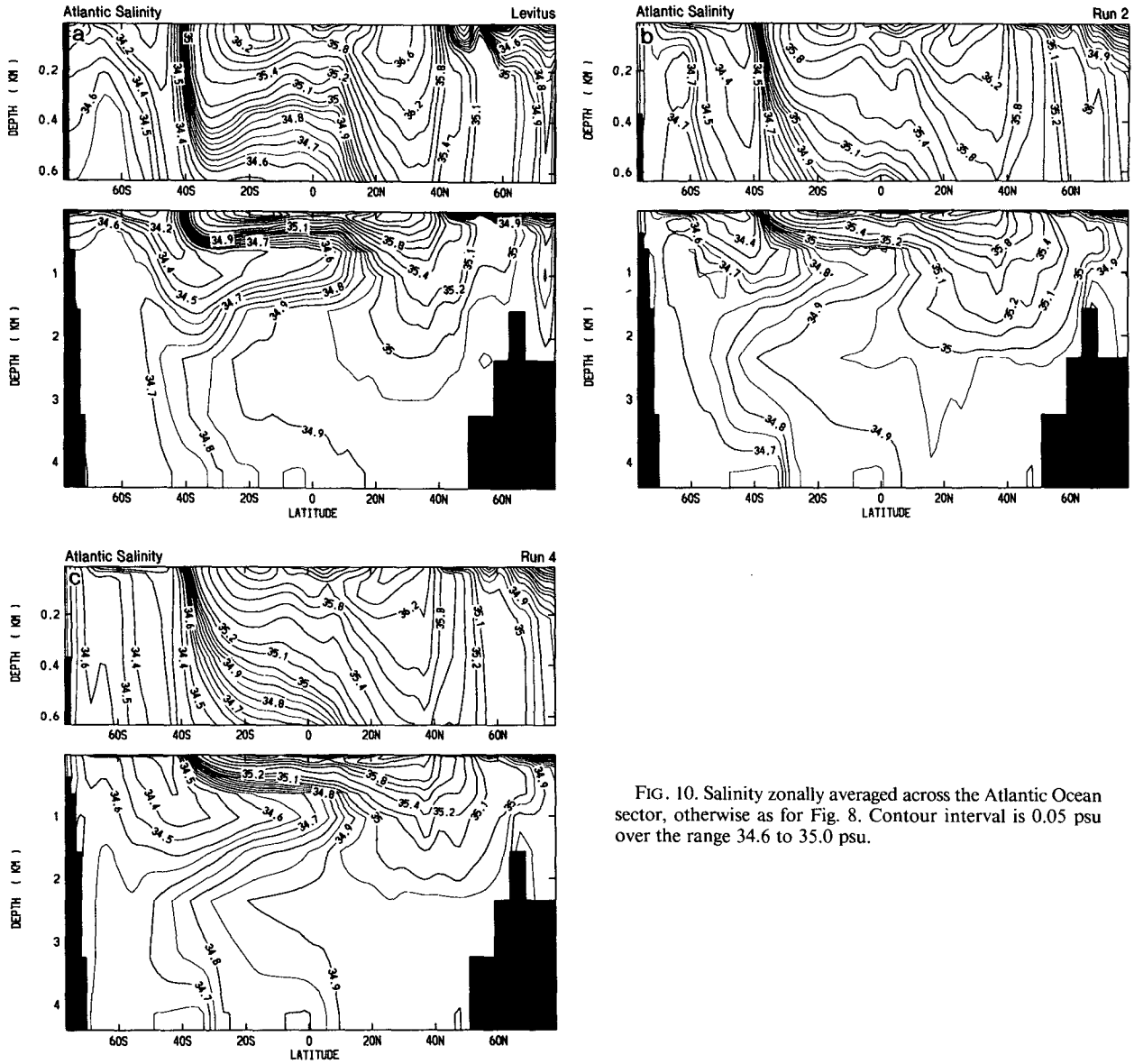

FIG. 10. Salinity zonally averaged across the Atlantic Ocean sector, otherwise as for Fig. 8. Contour interval is 0.05 psu over the range 34.6 to 35.0 psu.

modest isopycnal diffusivity (A_{TI}) prescribed in run 3. Figure 11 shows that the isopycnal mixing of run 3 results in a general cooling and freshening at depths below about 300 m, relative to the run 2 solution. The changes are largest at intermediate depths. The stronger isopycnal mixing in run 4 causes additional freshening and cooling. As a result, the T–S curves for runs 3 and 4 are seen to be more realistic than those of run 2. In run 4, intermediate salinity minima approach realistic values; however, deep salinities in the Indian and Pacific become slightly too low.

The zonal averaged T and S fields for the ocean sectors in run 4 are shown in Figs. 8c–10c. Note in particular the stronger salinity minimum associated with AAIW in both the Pacific and Atlantic. However, the simulated Pacific salinity minimum still displays deficiencies in strength and structure. First, the minimum is too weak, especially south of 15°S. This result contrasts with that of England (1993), who found a very strong salinity minimum when using the same profile of isopycnal diffusivity. However, his experiments contained several significant differences to the present, for example, the method of polar deep water forcing and the values of other mixing coefficients. Second, the salinity minimum is too homogeneous across the tropical Pacific. This result appears consistent with the solution of England (1993) and suggests that the models are missing some significant large-scale feature that could involve vertical motion or latitudinal modulation of the diffusivities.

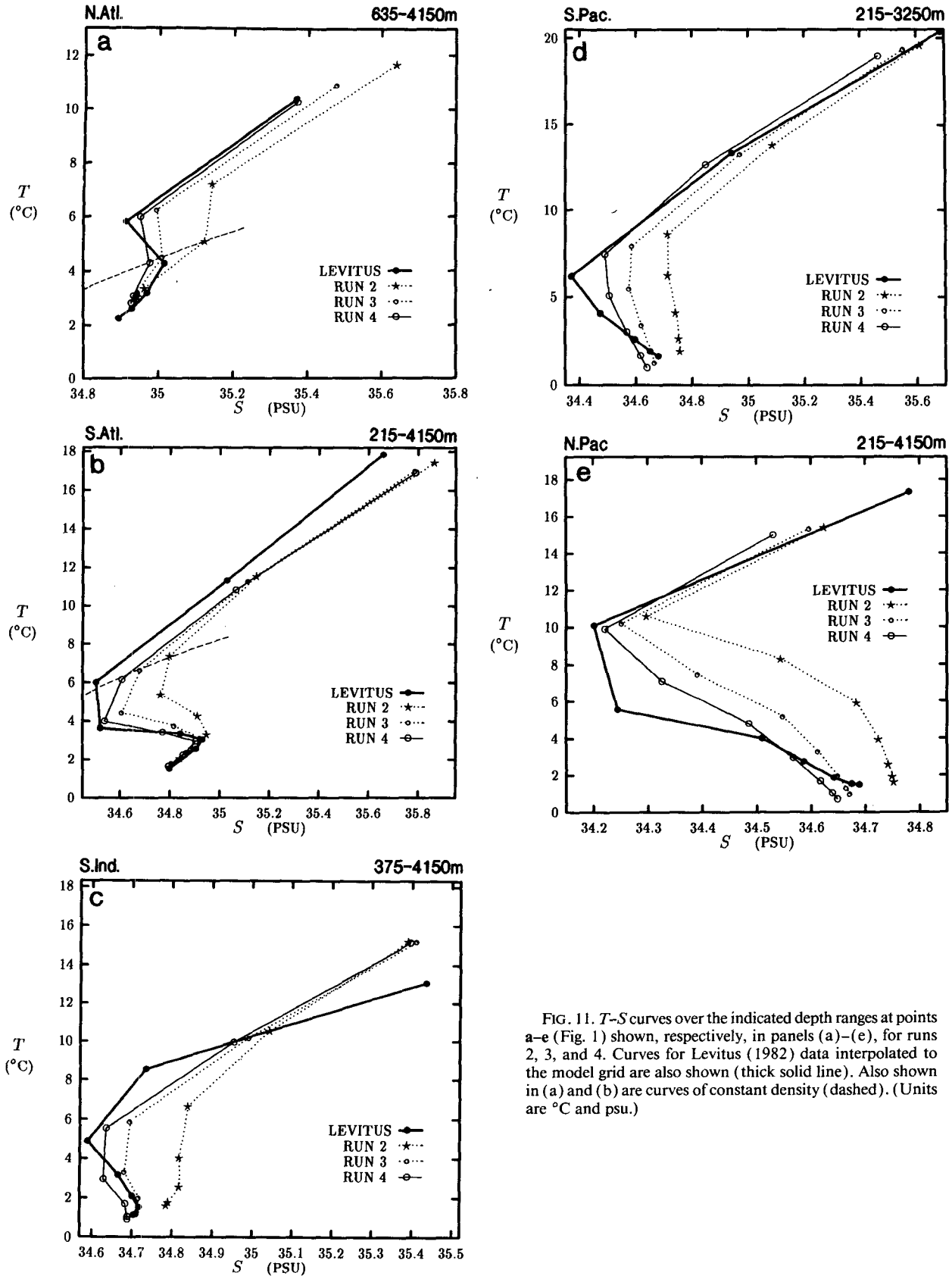

FIG. 11. T–S curves over the indicated depth ranges at points a–e (Fig. 1) shown, respectively, in panels (a)–(e), for runs 2, 3, and 4. Curves for Levitus (1982) data interpolated to the model grid are also shown (thick solid line). Also shown in (a) and (b) are curves of constant density (dashed). (Units are °C and psu.)

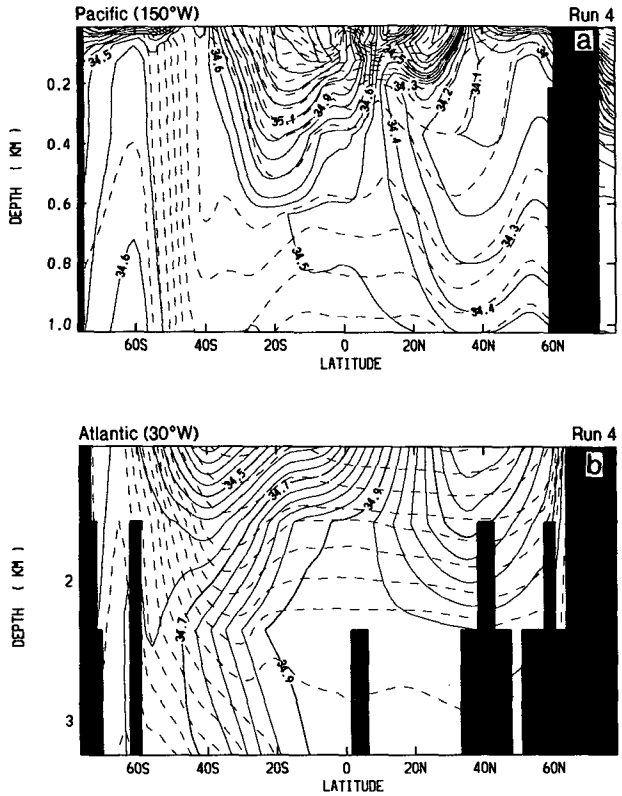

FIG. 12. Meridional sections of salinity (solid) and potential density (dashed) for run 4 for (a) the upper Pacific Ocean at 150°W and (b) the deep Atlantic Ocean at 30°W. Potential density reference levels are $z = 0$ and $z = 2350$ m depth, respectively. (Salinity has units of psu.)

The means by which the isopycnal mixing acts to enhance the AAIW salinity minimum is well illustrated in Fig. 12a. This meridional section from the mid-Pacific shows potential density (referenced to the surface) superimposed on the salinity field. The potential density contours give an approximate indication of the neutral surface orientation. There is little downward mixing of the fresh cold surface water poleward of about 60°S, since the neutral surfaces associated with the near-surface halocline there are almost horizontal. Further north, neutral surfaces slope steeply downward from the surface, with those surfaces originating from between 60°S and 53°S reaching particularly great depth. Isopycnal mixing allows the latter surfaces to act as pathways along which the fresh surface water may mix deep into the ocean interior. In the upper 90 m, the modest slope of these surfaces (about 1:5000) nevertheless implies a mixing rate projected onto the vertical of the same order as that provided by a vertical diffusivity of $[A_{TI} \times (\text{slope})^2 =] 2\ \text{cm}^2\ \text{s}^{-1}$, or 10 times the background value. At greater depth, the much larger slope of the neutral surfaces (typically about 1:300) implies mixing equivalent, in the same sense, to a vertical diffusivity of order 300 $\text{cm}^2\ \text{s}^{-1}$. Such large diffusivity would totally dominate any large-scale vertical motion, which may be expected as a result of surface Ekman divergence (as discussed by England et al. 1993). As a consequence, S gradients along the steeply sloping surfaces are very weak. Similar plots for run 2 reveal little change in the potential density field, but much greater S (and T) gradients occur along the steeply sloping surfaces.

The AABW and Circumpolar Deep Water (CDW) of the Southern Ocean tend to freshen as A_{TI} is increased (e.g., Figs. 9 and 10, Table 3). Isopycnal mixing is ineffective in mixing downward the high-salinity shelf waters of the Weddell and Ross Seas (cf. England 1993). In all the present runs, the shelf water mixes with much fresher water near the shelf margin (such as discussed in section 7 for the Ross Sea). The resulting water on the continental slope is fresher and colder than the deep water of the Southern Ocean, and it is this water that then may flow or be mixed downward.

The deep waters of the Indian and Pacific Oceans are also substantially fresher in those runs with isopycnal mixing. These waters are blends of salty NADW and relatively fresh Antarctic waters. The NADW outflow separates from the South American coast at mid-latitudes, and then flows generally eastward around the Southern Ocean, during which time it progressively mixes with the Antarctic waters. The resulting mixed water flows into the deep Indian and Pacific basins. Now, the NADW outflow entering the South Atlantic varies little in volume or salinity between the runs (Table 3). However, its subsequent mixing with the fresher Antarctic waters of runs 3 and 4 would be expected to result in Indian and Pacific deep water fresher than in run 2. Further, *additional* mixing along isopycnals occurs in runs 3 and 4. The direct effect of isopycnal mixing on the NADW outflow is illustrated in Fig. 12b, which shows potential density (referenced to 2350 m) and salinity for a meridional section in the mid-Atlantic. Clearly apparent are the (approximate) neutral surfaces extending downward and northward from the southernmost portion of the AAIW salinity minimum into the NADW salinity maximum. Such a configuration allows isopycnal mixing to directly dilute the outflowing NADW by, especially, fresh AAIW. Time scales of both horizontal and isopycnal mixing are crudely estimated to be of the same order as the advective time scale from South America eastward to south of the Pacific (the vertical mixing time scale is an order of magnitude longer). In any case, it is apparent that direct isopycnal mixing contributes to some extent to the relatively rapid eastward diminution of the NADW salinity maximum in the Southern Ocean evident in runs 3 and 4, and thereby to the interrun salinity differences in the deep Indian and Pacific Oceans. We note, however, that such water mass interaction via isopycnal mixing is very dependent on relative densities of the water masses involved, and is therefore likely to be highly model dependent.

We turn now to the effect of enhanced isopycnal mixing on the ocean's dynamics. The (T, S) values in Fig. 11 generally show a systematic shift toward fresher cooler water as A_{TI} is increased. At most points, this shift occurs with little change in potential density. By way of example, curves of constant potential density are shown in Fig. 11a for level 9 (1575 m) and in Fig. 11b for level 7 (635 m). The small departure of the respective (T, S) values from these curves is typical. On the larger scale, Fig. 4 shows that the mean stratification for runs 3 and 4 is little changed from that in run 2. Clearly, the large T and S changes induced by isopycnal mixing have only minor effect on the density fields. We do note that isopycnal mixing may alter density directly via cabbeling and thermobaricity (McDougall 1987b). Further, isopycnal mixing may alter the T/S characteristics of water at one depth, which, after advection to another depth, will acquire an altered density as a result of the different pressure dependencies of the T and S expansion coefficients. Such effects here appear to be minor, on the large scale.

The minimal changes in the large-scale density fields between runs 2, 3, and 4 result in minimal changes in the current structure. Figure 5 shows that the vertical structure of the tropical/midlatitude currents is almost totally insensitive to the degree of isopycnal mixing. The ACC strengthens slightly with increased isopycnal diffusivity (Table 3), in association with small increases in deep water density near Antarctica. The meridional overturning streamfunctions for runs 3 and 4 are found to be almost identical to those for run 2 in Fig. 6.

Finally, we note that isopycnal diffusion induces a modest increase in poleward heat transport in the midlatitude Southern Hemisphere (Fig. 7). This increase appears associated with enhanced isopycnal mixing of warm, salty water from the subtropical gyre with cooler, fresher water further to the south. The resulting changes in heat and salt transports counterbalance so as to leave buoyancy transport relatively unchanged.

c. *Reduced deep ocean isopycnal diffusivity*

Run 5 examines the effect of reducing A_{TI} at depth while maintaining the same surface value as in run 4 (Fig. 2b). The T, S response at point b in the South Atlantic and point d in the South Pacific are shown in Fig. 13. The South Atlantic values are almost unchanged. In the South Pacific, the only noticeable change is a very slight increase in salinity (by $\sim$ 0.02 psu) below about 1500 m. Such a response is typical of that found elsewhere in the Pacific and Indian basins. Some increase in the deep Pacific and Indian salinities may be expected, given the potential of isopycnal diffusion to modify NADW outflow as discussed earlier. Nevertheless, we conclude that the T and S fields are rather insensitive to the prescribed deep values of A_{TI}.

On comparing the results of runs 2–5, it is evident that the T and S fields generally are sensitive to the near-surface values of A_{TI}, in some cases more than to the local value. In particular, salinities at the intermediate salinity minimum decrease markedly between runs 3 and 4, when both local and near-surface A_{TI} are increased, yet remain almost unchanged between runs 4 and 5, when local A_{TI} is reduced while near-surface A_{TI} remains constant (cf. Figs. 11, 13). Isopycnal gradients of S at the salinity minimum are typically very small in all of runs 3–5 (e.g., Fig. 12a), and so moderate local changes in A_{TI} would be expected to have little effect on the salinity minimum (even if the minimum were being maintained solely by isopycnal mixing). In contrast, Fig. 12a shows rapid change in S along the isopycnals within 100 m of the surface in the AAIW

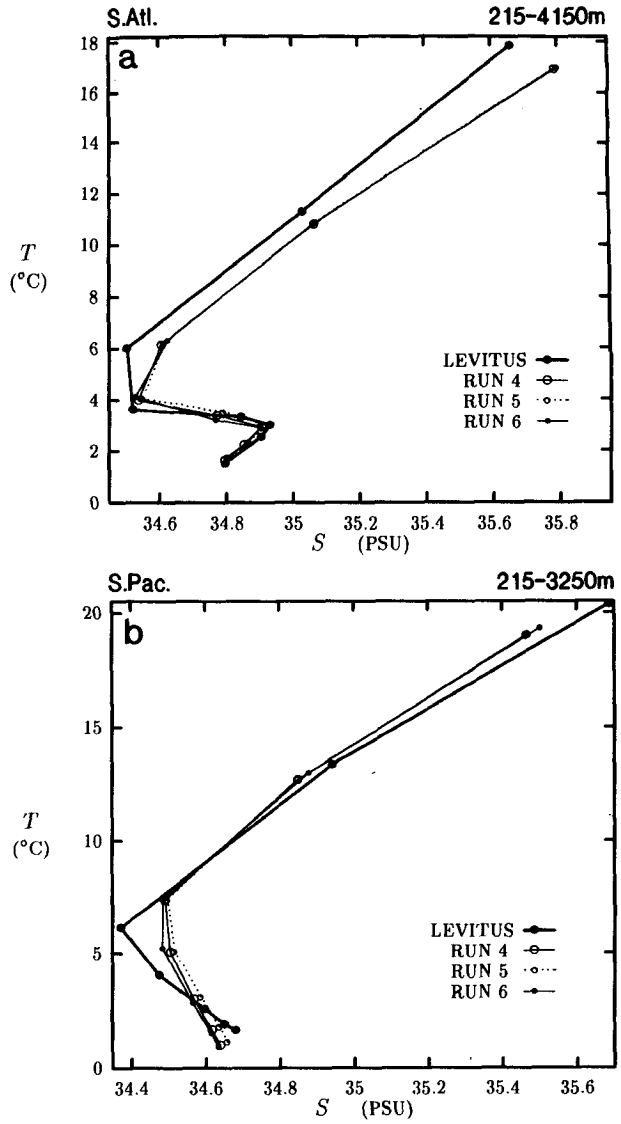

FIG. 13. T–S curves over the indicated depth ranges at (a) point **b** in the South Atlantic, and (b) point **d** in the South Pacific (Fig. 1), for runs 4, 5, and 6, and for Levitus (1982) data interpolated to the model grid.

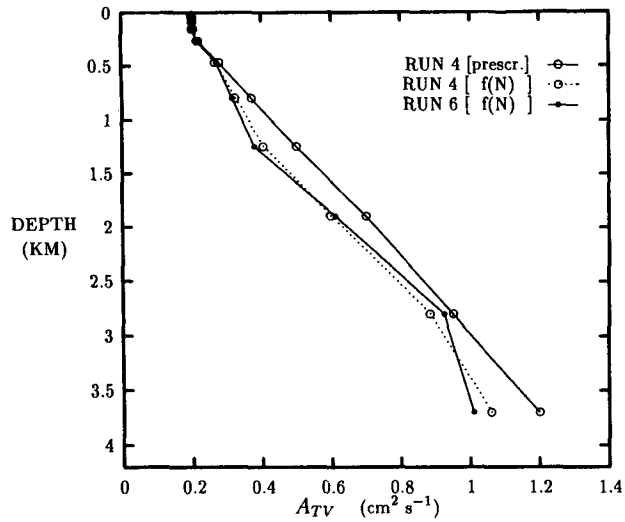

FIG. 14. Profiles of "effective large-scale vertical diffusivity" A_{TV}^{eff}, as defined in the text, for runs 4 and 6. Also shown is the A_{TV}^{eff} profile that would result if Eq. (2) were applied to the T and S fields of run 4. (Units are cm^2 s^{-1}.)

source region, which presages high sensitivity of the salinity minimum to change of *near-surface* A_{TV}.

d. Stability-dependent vertical diffusivity

This section examines the effect of setting the vertical diffusivity to be dependent on static stability. Results are presented from run 6, which is identical to run 4 except that A_{TV} is made proportional to $(1/N)$ as per (2). Therefore, A_{TV} becomes a diagnostic model variable that varies spatially and temporally. Since the model's stratification (thus N) is in turn strongly dependent on the vertical diffusivity (e.g., section 5a), the potential might exist for large changes in the model solution to occur in response to introduction of the parameterization (2) (e.g., Gargett 1984). A comparison with the run 4 solution reveals that such large changes do not occur. For example, T and S values at points **b** and **d** are little changed (Fig. 13), as are essential circulation parameters (Table 3). Meridional heat transports differ from those of run 4 by less than 3%.

The surprising lack of change upon adoption of a diagnostic A_{TV} is explained with reference to Figs. 14–16. Figure 14 compares the profiles of "effective large-scale vertical diffusivity" (A_{TV}^{eff}) for runs 4 and 6, where A_{TV}^{eff} is defined

$$A_{TV}^{\text{eff}} = \frac{\iint |A_{TV} T_z| \, dxdy}{\iint |T_z| \, dxdy}, \tag{4}$$

that is, the average magnitude of vertical diffusive heat flux divided by the average magnitude of vertical temperature gradient. For Fig. 14, the area of integration is over all ocean regions between 45°S to 45°N. Points experiencing convective mixing are excluded from the calculation. We prefer A_{TV}^{eff} as a measure of vertical diffusivity over, say, a simple area average of A_{TV} because the latter is severely biased upward in run 6 by a few points, which have very large A_{TV} but make rather small contribution to the vertical heat and salt flux as a result of locally weak vertical gradients. The profile of A_{TV}^{eff} in run 4 is of course identical to the prescribed profile of A_{TV} (Fig. 2a). The profile of A_{TV}^{eff} in run 6 is quite similar to that in run 4, with values below 500 m depth generally showing a small reduction.

Unlike in run 4, A_{TV} in run 6 displays significant meridional variation. Shown in Fig. 15 is the "effective zonally averaged vertical diffusivity" (A_{TV}^{za}) defined by

$$A_{TV}^{\text{za}} = \frac{\int |A_{TV} T_z| \, dx}{\int |T_z| \, dx}. \tag{5}$$

For Fig. 15, the zonal integration is conducted across the Pacific region shown in Fig. 1. Equatorward of about 30° latitude, the profile of A_{TV}^{za} is fairly uniform and resembles that shown in Fig. 14. Poleward of 40°S, A_{TV}^{za} increases at all levels, as the static stability weakens markedly. Broadly similar results are found for the other ocean basins, though the A_{TV}^{za} for the North Atlantic also increases poleward, especially from about 40°N.

Given that A_{TV} in run 6 differs only modestly from that in run 4 over most of the domain, it is to be expected that the model solutions also differ little. The primary reason for the similar A_{TV} values in the upper ocean is simply that the upper ocean A_{TV} for run 6 generally defaults to the lowest allowed value of 0.2 cm^2 s^{-1}, which is just the same as the upper ocean A_{TV} prescribed for run 4. It is well known that upper-ocean A_{TV} strongly controls pycnocline depth and meridional heat transport.

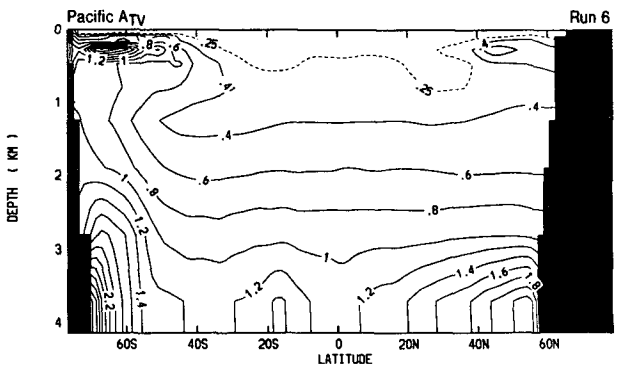

FIG. 15. "Effective zonally averaged vertical diffusivity," as defined in the text, for the Pacific sector for run 6. (Units are cm^2 s^{-1}.)

At greater depth, the prescribed deep ocean A_{TV} values in run 4 are based on observed stratification (via Kraus 1990), and we note that the run 4 solution achieves fairly realistic stratification (Fig. 4). Therefore, when we apply the same formula as Kraus (1990) to calculate A_{TV} in run 6, it is no surprise that the A_{TV} values do not change greatly from those prescribed in run 4. Also shown in Fig. 14 is the A_{TV}^{eff} that would result from applying (2) to the run 4 density field. The small difference between this curve and the actual prescribed profile foreshadows the generally small change in A_{TV} attained between runs 4 and 6.

There is no evidence of any positive feedback involving A_{TV} and stratification, which could lead to large differences between the run 4 and 6 solutions. In fact, Cummins (1991) has shown that there may be instead a negative feedback, where increased A_{TV} at depth leads to increased meridional overturning, which actually strengthened the deep stratification. Thus A_{TV} computed via (2) would then decrease. Such a feedback would tend to limit the differences between solutions with prescribed and calculated A_{TV}.

In the subpolar regions, A_{TV} profiles in run 6 are typically not like that in run 4, yet this change little affects the solution. An explanation for this result is provided by Fig. 16, which shows latitude–depth sections of the diapycnal diffusivity ratio (DDR) as defined by Cummins et al. (1990), DDR = A_{TH}^{*}/A_{TV}, where $A_{TH}^{*} = A_{TH}m^2$ and m is the isopycnal slope. For $m \ll 1$, this quantity gives the ratio of diapycnal diffusion associated with the (artificial) horizontal diffusivity to that associated with the vertical diffusivity. Vertical diffusivity is dominant over most of the ocean (DDR $\ll 1$), but, in the subpolar regions, horizontal diffusivity dominates by more than an order of magnitude. This dramatic increase in DDR reflects the relative steepness of the isopycnal slopes common in the subpolar regions. In such regions, the dominant balance in the buoyancy budget is between advective terms and horizontal diffusion. Modest changes in the vertical diffusion term, such as resulting from the modest A_{TV} changes between runs 4 and 6, would have little effect on the overall buoyancy budget, and therefore have little effect on the stratification and circulation.

Cummins et al. (1990) found relatively large changes in their deep ocean behavior when they changed from a uniform prescribed A_{TV} to a A_{TV} based on (2). However, their prescribed value of A_{TV} of 0.1 cm^2 s^{-1} was much smaller than that which would be calculated via (2) given the very weak deep stratification present in that run. In such a case, substantial adjustment in the solution would be expected upon change to calculated A_{TV}.

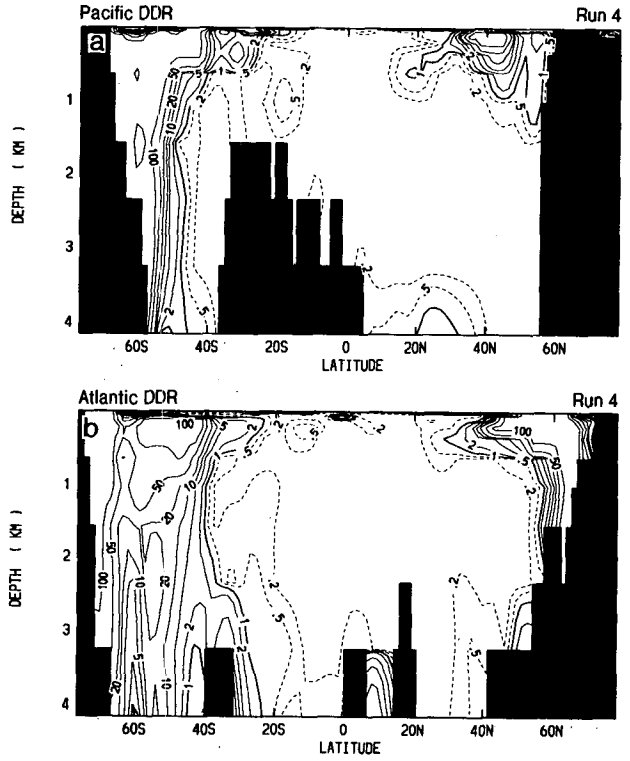

FIG. 16. Sections of diapycnal diffusivity ratio (DDR), as defined in the text, for (a) Pacific at 160°E and (b) Atlantic at 35°W, for run 4.

6. Results of additional runs

a. Effect of horizontal diffusivity

The model numerics require retention of a background horizontal diffusivity (A_{TH}) in all runs. In the vicinity of sloping neutral surfaces, this unphysical diffusivity can be dominant in the diapycnal diffusion of buoyancy and scalars (e.g., section 5d). Here, we test the robustness of the results from section 5, with respect to variation in A_{TH}, by examining the solutions of three runs where A_{TH} is set to be *double* the standard value. The runs, denoted runs 2h, 4h, and 6h, are otherwise identical to runs 2 (no isopycnal diffusivity), 4 (large isopycnal diffusivity), and 6 (large isopycnal diffusivity and stability-dependent A_{TV}).

Figure 17 shows T, S curves at points **b** and **d** for the three runs. On comparing with Figs. 11 and 13, the effect of increased A_{TH} is seen to be rather small. Inspection of large-scale S fields indicates that, overall, increased A_{TH} is associated with slightly reduced contrast between the different water masses. However, the general differences in water mass structure between runs 2, 4, and 6 are preserved.

Increasing the A_{TH} has some effect on oceanic circulation and meridional heat transport. The ACC and the Atlantic overturning circulation are moderately weakened (Table 3). Meridional heat transport is more southward by 0.1–0.3 PW at all latitudes from 40°N to 60°S because of the weaker Atlantic circulation and because of increased diffusive heat transfer in the vi-

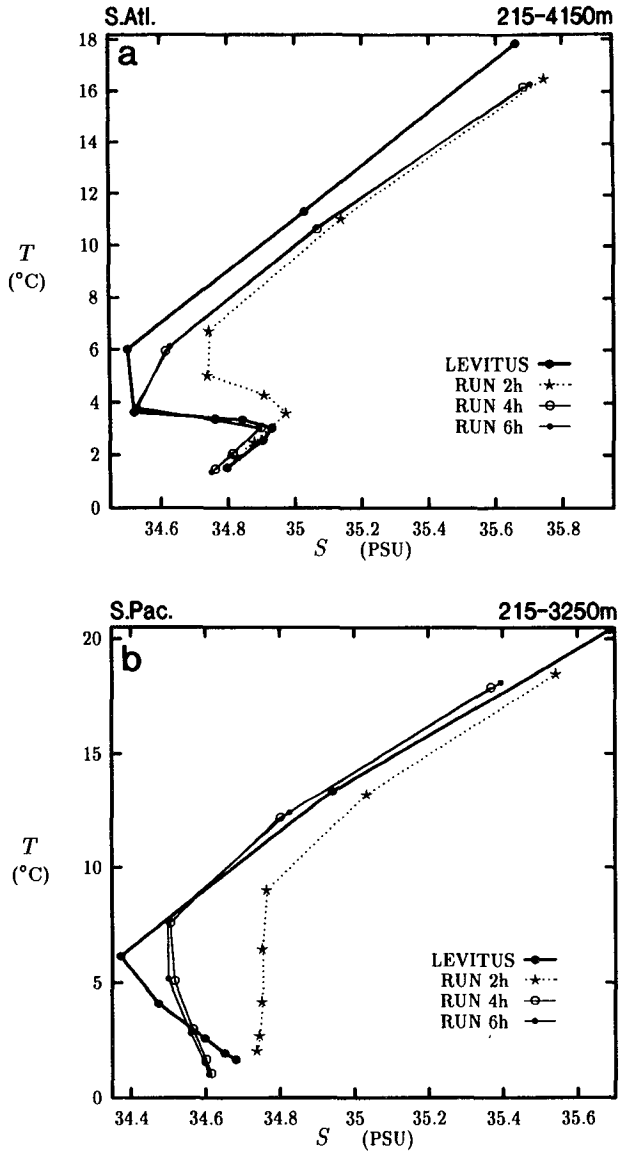

FIG. 17. T–S curves for runs 2h, 4h, and 6h, otherwise as for Fig. 13.

cinity of the ACC. Again, however, the general results regarding currents, stratification, and heat transport between runs 2, 4, and 6 are found to be preserved. We conclude that the interrun differences discussed in section 5 are insensitive to moderate changes in A_{TH}.

b. *Effect of enhanced near-surface mixing*

Another deficiency of the present model is the lack of parameterization for wind-forced mixing and solar penetration. This deficiency is the probable cause of the tendency for model density to increase too rapidly with depth in the layers immediately beneath the surface, as evidenced in Fig. 4. In this section, we examine the robustness of our earlier results with respect to enhanced surface mixing. Runs 2, 4, and 6 are rerun simply with a larger prescribed vertical diffusivity between the uppermost layers. The new runs are referred to as runs 2ml, 4ml, and 6ml, respectively, where the suffix "ml" refers to upper "mixed layer." Near-surface A_{TV} is altered such that the upper density profile for the solution averaged between 60°N and 60°S is very close to the observed. Namely, values of A_{TV} between the top four layers are increased by 1.8, 0.8, and 0.2 $cm^2\ s^{-1}$, respectively, over the entire ocean domain. The resulting average profile of density for run 4ml is compared with that of run 4 in Fig. 18. Average profiles for runs 2ml and 6ml are similarly realistic. This method of representing surface mixing is of course extremely crude and neglects the effects of horizontal variation in governing fields such as wind stress. Our aim here is to explore only the potential zero-order effects of surface mixing on the model solution as a whole.

Figure 19 shows T, S curves at points **b** and **d** for runs 2ml, 4ml, and 6ml. Enhanced surface mixing results in freshening and cooling at intermediate and (to a lesser extent) deep levels. These changes are greater in the presence of isopycnal mixing than in its absence. NADW properties and outflow volume (Table 3) change little between the runs, so are not responsible for the above differences. Rather, there is a general freshening and cooling of Antarctic waters. A change in Pacific deep-water properties then presumably occurs as a result of mixing of NADW outflow with the fresher, colder Antarctic waters.

The different effect of enhanced surface mixing on the NADW and Antarctic water masses may be explained in terms of the near-surface T and S profiles

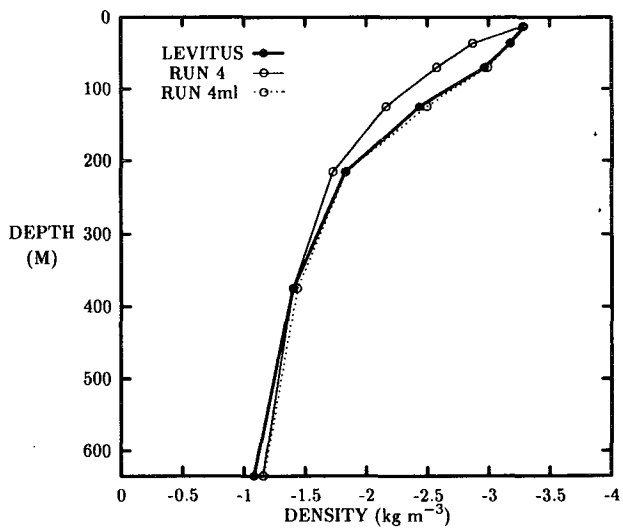

FIG. 18. Profiles of density ($\sigma_{s,t,p} - \sigma_{35,0,p}$) in the upper ocean, averaged between 60°N and 60°S, for runs 4 and 4ml, and for Levitus T and S (interpolated to model grid). (Units are kg m^{-3}.)

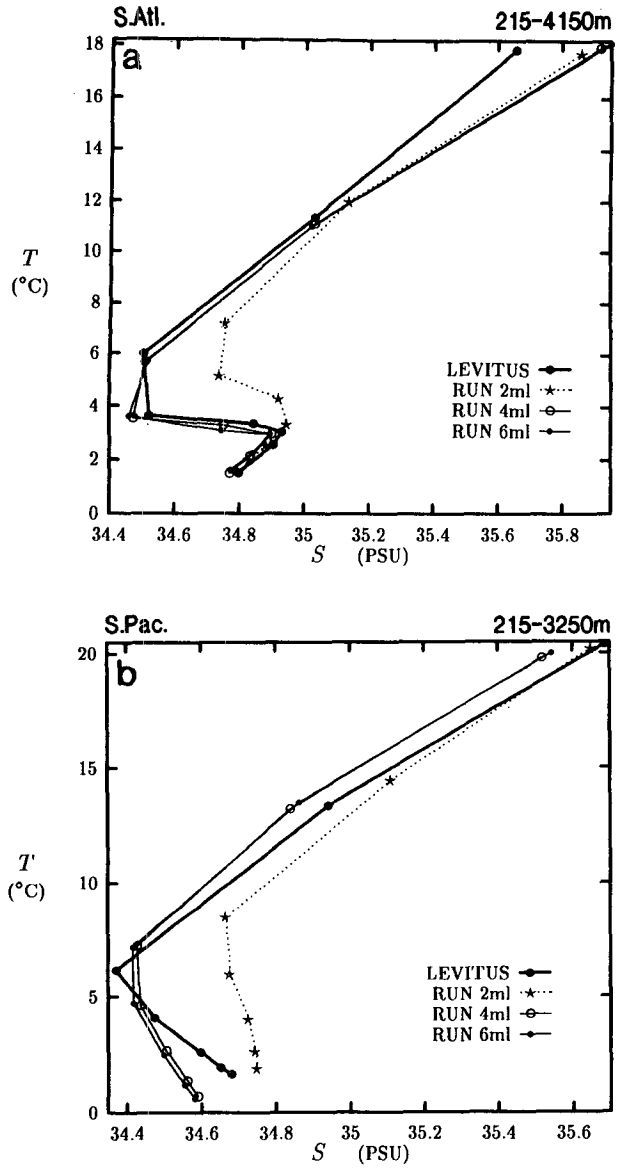

FIG. 19. T–S curves for runs 2ml, 4ml, and 6ml, otherwise as for Fig. 13.

characteristic of the water mass source regions. Much of the North Atlantic Ocean, Labrador Sea, and Norwegian/Greenland Sea are characterized by strong surface cooling and thus convective and/or steep isopycnal mixing. Such mixing results in weak vertical gradients of T and S near the surface. An additional surface mixing would then have only a minor effect on the T and S fields, and thus NADW. In contrast, the vast majority of the ocean surface near Antarctica is dominated by very cold and fresh surface water. This water is lighter than the warmer and saltier water below, and, in the absence of enhanced surface mixing, a pronounced halocline forms at the base of the first model layer. Enhanced surface mixing considerably deepens this halocline (bringing it closer to the observations), and facilitates greater participation of the fresh surface water in formation of Antarctic water types.

The most important result here is that the effects of isopycnal mixing and stability dependence of A_{TV} on the model solution are qualitatively the same whether or not enhanced surface mixing is included. The effect of isopycnal mixing on water mass properties is simply accentuated in the case where enhanced surface mixing is included.

c. *Effect of full annual cycle forcing*

In this section, we examine the extent to which the solution is affected by a change of upper forcing from perpetual winter in T and S to a full annual cycle. Increased computation prevents us from performing more than one such experiment, and we chose the model version used in run 5 (large surface/weak deep isopycnal mixing) since we judged it to yield the "most realistic" water masses when forced with perpetual winter conditions (section 5c). The annual cycle run will be referred to as run 5s.

In run 5s, the model is forced with the full annual cycle of Hellerman and Rosenstein (1983) wind stress. Between 1 February and 10 April of the model year, the surface layer T and S fields were relaxed toward March climatology (i.e., February–April for S) from Levitus (1982), together with wintertime corrections for the *Northern Hemisphere* as detailed in section 3. Between 1 August and 10 October of the model year, the surface-layer T and S fields were relaxed toward September climatology, together with wintertime corrections for the *Southern Hemisphere.* Thus the forcing in the Northern Hemisphere during the former, and the Southern Hemisphere during the latter, period is identical to that applied during the perpetual winter runs. During the transition seasons, the relaxation T and S fields on 5 December and 5 June are set to the December and June climatologies, respectively. Relaxation fields at other dates are calculated via linear interpolation between these transition fields and the nearest peak season fields. The corrections to the wintertime fields are not included in the interpolations during the early warming season, so as to simulate rapid early spring cessation of dense water formation. The e-folding time scale for surface relaxation is shortened to 2 days, which allows wintertime surface densities in key polar water formation regions to approach values obtained under perpetual winter conditions. (A relaxation time scale of 4 days would imply an e-folding adjustment time of 128 days for a typical well-mixed water column of 800 m depth, which is much longer than the 70 days of applied full winter forcing, resulting in incomplete adjustment.)

The time-stepping procedure was initially similar to that used for run 5, namely, using the full acceleration factors (section 4). However, a change in the time

stepping to uniform 1-day steps for T and S resulted in significant changes in the large-scale deep T and S trends. The perpetual winter runs did not display such large changes in the trends. These changes could result from interaction between the acceleration techniques and the annual cycle, since use of these techniques is known to be not strictly valid for integrations involving a final time-varying component (Bryan 1984). In any case, we abandoned the depth-dependent time stepping after 72 000 steps (200/1600 years) and ran the model for a further 150 years with a uniform one-day T–S time step, and then an additional 200 years with uniform half-day T–S time steps, to verify consistency of trends. At this point, globally averaged S values were satisfactorally converged (section 4). Some temperature drift rates were larger than the convergence criterion by a factor of two, but were declining steadily with time, and we elected to end the run.

We stress that the biases apparently introduced by the full acceleration factors do not appear to be particularly large. For example, examination of convergence rates for the above integration suggest biases in the converged deep salinities of order 0.02–0.04 psu. For most applications, such small biases are of little concern, and might be reduced by use of smaller acceleration factors. However, such biases are significant for studies attempting careful simulation of water masses, such as here.

Figure 20 shows T–S curves at points b and d for runs 5 and 5s. Introduction of the annual cycle results in only a small warming through the depth of the ocean. Deep salinities are slightly reduced. The freshening of the deep ocean is not uniform; NADW salinities are little changed, whereas deep salinities in the Weddell Sea are considerably lower (Table 3). The freshness of the Antarctic water appears linked, in turn, to excessive mixing of HSSW with fresher cold water types on and near the continental shelf. Consequently, HSSW displays a significant annual cycle in salinity (of order 0.05 psu amplitude), with an annual mean considerably lower than that under perpetual winter forcing. (We suspect that the real HSSW and Weddell Sea Bottom Water are less affected by the annual cycle.) Overall, however, the changes in the T and S fields between runs 5 and 5s are rather small, especially when compared to those fields resulting from models under annual-mean forcing (e.g., Toggweiler et al. 1989a; HG).

The meridional overturning streamfunction and the meridional oceanic heat transport are little affected by the switch to annual cycle forcing. Plots of meridional overturning streamfunction averaged over the final year of run 5s are almost identical to those for runs 2–5 (see also Table 3). The final-year average of global meridional heat transport differs from that of run 5 by mostly less than 0.1 PW.

We have verified that surface restoration of T and S to perpetual winter values produces a solution differing only slightly from that produced by use of a full

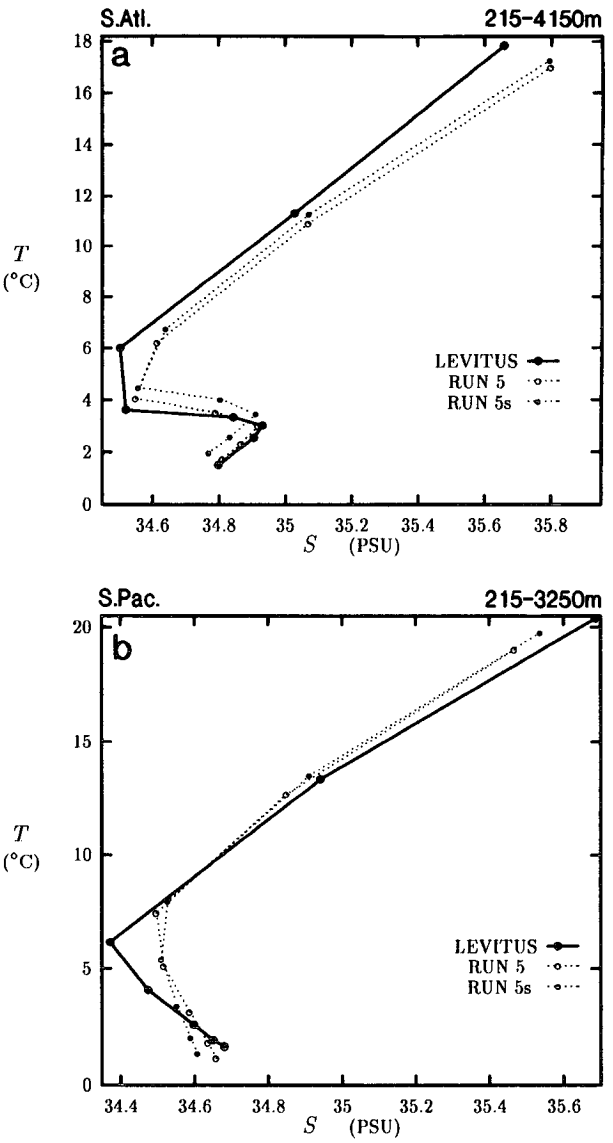

FIG. 20. T–S curves for runs 5 and 5s, otherwise as for Fig. 13.

annual cycle, in terms of the large-scale properties examined in this study. Comparison with results from other studies indicates that restoration to perpetual winter values will yield water masses that are more realistic than restoration to annual mean values. Therefore, we recommend restoration to perpetual winter values for those studies where temporally constant restoration fields are desired. One motivation for using such fields is to avoid the possibility that accelerated-convergence techniques may introduce biases upon interaction with an annual cycle. While the run 5s results suggest that any such biases are rather small, and no greater than the changes induced by replacing annual cycle with perpetual winter restoration, the possibility of run-to-run variation in the bias can complicate interpretation of model experiments.

7. Comments on model deep water and its formation

The deep water T, S characteristics in a global ocean model are determined by the interleaving and mixing of water masses from several sources. Errors in the densities of newly formed deep water masses are likely to affect the subsequent pattern of interleaving, and also the degree of mixing between the water masses along neutral surfaces. Such errors could result in significant errors in the deep ocean ventilation rate, with adverse consequences when the model is used for tracer and climate change work. Therefore, a few comments on the present model's formation of deep water are appropriate.

In reality, much of the deep water is believed formed from downslope flows of very dense water (e.g., down the Antarctic continental slope, or following shallow-sill outflow from the Greenland/Norwegian Sea) (Killworth 1983). Such flows typically have a depth of no more than a few hundred meters (e.g., Swift 1984; Saunders 1990) and proceed down slopes with aspect ratio of order 1:100, giving an effective horizontal scale of a few tens of kilometers. Clearly, coarse-resolution models on an (x, y, z) grid will be unable to properly simulate such flows. An example from the present model is the immediate and unrealistic obliteration of the western Ross Sea salinity maximum upon reaching the edge of the continental shelf. In the model, a 2 Sv flow of cold and salty shelf water proceeds northward in the bottom layer (470–800 m depth), then over the shelf edge to the next grid box where the floor is at 1900 m. There, convection ensues from 470 m to the floor. Entering into this convecting column is a 5 Sv flow of water from the east, which has been freshened by nearby open-sea convection. The two water masses mix completely in the convecting column. In reality, the high salinity water slides down the slope under any less dense long-slope current (Gordon 1975). Some mixing occurs, but not the *total* mixing guaranteed in the present model.

Alternative numerical formulations (e.g., Oberhuber 1993; Gerdes 1993) might offer some improvement in the representation of deep water formation, but the fundamental problem of degree of mixing remains. This is because the observed dilution rates of downslope flows appear strongly influenced by subgrid-scale factors such as local topographic variation (e.g., Swift 1984; Saunders 1990). While it may be possible to devise a parameterization to represent downslope-flow and its mixing in a particular GCM, it is likely that the coefficients involved would have to be separately tuned for each downslope flow, based on the observed degree of mixing.

Given the unphysical and uncontrolled mixing of downslope flow in the present model, it is worth considering how the present runs are able to produce NADW with fairly realistic T and S. The observed sill overflow of dense Greenland/Norwegian Sea water occurs at several locations, both east and west of Iceland, with an estimated total volume of 3.5–5.5 Sv (e.g., Swift et al. 1980; Saunders 1990). In the model, the overflow (of 6.5 Sv below 470 m depth) is almost totally confined to the model's Denmark Strait, west of Iceland. The equal depth (800 m) of the eastern and western sills in the model may contribute to this discrepancy; in reality, the Denmark Strait sill is about 200 m shallower. The model's Denmark Strait overflow displays fairly realistic properties (e.g., 0.61°C/34.880 psu in run 4). It appears that unrealistic concentration of all dense water overflow to the Denmark Strait allows for dilution in the model to be reduced toward realistic levels.

Realistic simulation of NADW density appears to be especially important for successful simulation of the global-scale water masses. In some preliminary runs, with only a shallow (250 m) Denmark Strait and/or without the Labrador and Greenland Sea wintertime corrections, resulting NADW was rather less dense than for the present runs. In association with the reduced density, NADW outflow was shallower and weaker, AABW penetrated more strongly into the North Atlantic, and the effect of NADW outflow on the Indian, Pacific, and Southern Oceans was reduced. Consequently, the latter, remote, ocean basins experienced lower deep salinities and temperatures.

Toggweiler and Samuels (1993) recently presented model results supporting the hypothesis that NADW outflow from the Atlantic is controlled by the strength of the circumpolar winds at Drake Passage latitudes. However, in the course of the preliminary experiments noted above, we found that the NADW outflow volume was strongly dependent on the density of NADW (relative to other intermediate/deep water masses). For an extreme case, we may compare the Atlantic circulation found by HG (their Fig. 7a) to that of run 1 (Table 3). The former featured annual-mean T/S forcing and a shallow Denmark Strait, and yielded light NADW with a net outflow of 9 Sv. The latter features corrected wintertime T/S forcing and a deep Denmark Strait, yielding denser NADW and an outflow of 21 Sv. This difference is despite identical wind forcing and Southern Ocean topography, and nearly identical model parameters. Apparently, the strength of NADW outflow is dependent partly on the Southern Hemisphere winds and partly on the strength of effective buoyancy forcing in the North Atlantic. A similar conclusion was reached by England (1993).

8. Summary and concluding remarks

This paper explores the impact of several physically based enhancements in subgrid-scale mixing parameterization on the solution of a global ocean GCM. Results are presented from a series of model runs in which the improved parameterization is introduced step by step in order to clearly evaluate the effect of each

change. The surface forcing is held the same for all principal runs, and features a strong relaxation of surface T and S toward *perpetual wintertime* observed values. One of the model versions is rerun with a full annual cycle to verify that essential model characteristics (mean meridional heat transport and overturning circulation, and subsurface water mass properties) are little affected by the use of perpetual winter surface T and S (section 6c).

The use of perpetual winter T and S results in considerable improvement in deep water properties over the commonly used annual-mean fields. NADW outflow volume is enhanced ($\sim$16 Sv) and its temperature and salinity are fairly realistic ($S \sim$ 34.9 psu). Northward penetration of AABW in the Atlantic is realistically weak. Deep salinities vary from the South Atlantic to the Indian to the Pacific, in qualitatively realistic fashion. Deep Pacific salinities (below 2800 m depth) fall mostly within the range 34.58–34.76 psu (compared to the observed 34.65–34.72 psu). Deep Pacific temperatures display a similar degree of realism.

Runs 1 and 2 examine the effect of changing the profile of vertical diffusivity from a uniform 1 $cm^2\ s^{-1}$ to a profile featuring a small upper-ocean value of 0.2 $cm^2\ s^{-1}$. Changes in meridional overturning, heat transport, and density structure broadly mirror those found in earlier work. Water mass properties in both runs are rather poor. In particular, the salinity minima of the intermediate waters are either weak or absent.

The salinity structure is much improved by the inclusion of parameterization for isopycnal mixing, in runs 3–5. Each of these runs features a different vertical profile of isopycnal diffusivity. Despite large changes in the T and S structure, the *density* structure and currents are little affected by the isopycnal mixing. Meridional heat transport is modestly increased in the midlatitudes (by up to 20%), apparently as a result of enhanced meridional mixing of warm salty subtropical water with colder fresher polar water, along the isopycnals.

The introduction of isopycnal mixing generally cools and freshens the intermediate and deep waters of the World Ocean. Intermediate water properties appear particularly sensitive to the near-surface value of isopycnal diffusivity, which controls the rate at which fresh cold surface water is mixed downward near the polar fronts. All the observed major intermediate salinity minima are present in all runs where isopycnal mixing is included and their strength increases as upper-ocean isopycnal diffusivity is increased. The deep water properties of the Southern, Indian, and Pacific Oceans are also fairly sensitive to the degree of isopycnal mixing, with Pacific deep salinity falling from about 34.75 in run 2 (no isopycnal mixing) to about 34.64 in run 4 (largest prescribed isopycnal diffusivity). The properties and outflow of NADW are little changed between the runs, and the deep water changes appear related to changes in the T–S characteristics of the Antarctic water masses and in the rate of mixing between the NADW outflow and these fresher water masses.

In run 6, we set the *vertical* diffusivity to be inversely proportional to the Brunt–Väisälä frequency (after Gargett 1984; Cummins et al. 1990), while using the same isopycnal diffusivities as for run 4. Little change is found in the solution from that of run 4. Factors contributing to the similarity of results are discussed in section 5d. In particular, the A_{TV} profile prescribed in run 4 happens to be quite similar to the depth dependence of A_{TV} typical of the tropics and midlatitudes in run 6.

We performed, in addition, two series of runs to examine the potential impact of specific model imperfections on the solutions. In the first series, we reran runs 2, 4, and 6 with horizontal diffusivity *doubled,* in order to explore the potential effect of the artificial horizontal diffusivity, which is retained for numerical reasons. In the second series, we again reran runs 2, 4, and 6, this time with vertical diffusivity increased between the upper four levels, to explore the gross effect of enhanced surface mixing. In both cases, changes to the respective solutions were fairly minor. Most importantly, the major differences and similarities between the solutions of runs 2, 4, and 6 were preserved, providing some confidence as to the robustness of the results discussed above.

Several aspects of the present solutions warrant further study. In particular, all model runs produce South Atlantic and North Pacific Intermediate Water with distribution qualitatively resembling the observed. The inclusion of strong isopycnal mixing and enhanced surface mixing allows these two water masses to appear quantitatively quite realistic (e.g., Fig. 19a). In contrast, the AAIW salinity minima in the model's South Pacific and Indian Oceans are more sensitive to change in mixing parameterization, are typically weaker than observed, and display significant errors in distribution. These latter water masses appear more fundamentally dependent on isopycnal mixing processes. A comparison of the thermohaline dynamics of the several intermediate waters in the model would be of interest.

The large effect of isopycnal mixing on the T and S fields indicates the importance of parameterizing this process as correctly as possible, in studies concerned with oceanic tracer distributions. Yet the present parameterization is deficient in several respects. For example, the assumption of horizontally constant isopycnal diffusivity is unrealistic, since it does not account for geographical variation in eddy behavior. At the very least, one might seek an expression of A_{TI} in terms of the large-scale model fields.

One very important property of the ocean model, which is relevant to climate-change modeling but was not examined here, is the ability to sequester additional heat in an environment of gradually changing surface thermal forcing. The rate at which the ocean can sequester the heat determines its effectiveness in retarding

global warming. Lin (1988) found substantial changes in the transient thermal response of an idealized analytic ocean model upon introduction of isopycnal diffusion. The heat-sequestering ability of the present model versions will be examined in a subsequent study.

Acknowledgments. The authors would like to thank Drs. M. H. England, J. S. Godfrey, T. H. McDougall, and A. M. Moore for helpful discussions during the course of this work. Thanks also to Drs. A. E. Gargett, B. G. Hunt, A. M. Moore, J. I. Syktus, and an anonymous reviewer for constructive reviews of preliminary drafts. The computations were carried out on the CRAY-YMP4E/369 located at the University of Melbourne, Parkville, Victoria. This work was partly funded by the Wool Research Corporation of Australia.

APPENDIX

Numerical Problems

Weaver and Sarachik (1990) and Gerdes et al. (1991) have highlighted numerical problems that can result from use of realistically small A_{TV} in association with a coarse vertical grid. The problems stem from the tendency of the centered difference algorithm to produce nonphysical ripples in the scalar fields, which may lead to local violation of the second law of thermodynamics. Such local violation can lead to spurious water mass formation. Both increased horizontal and vertical diffusivity helps reduce the rippling effect, but increased isopycnal diffusivity does not help (Gerdes et al. 1991). Since we use realistically small A_{TV} and a modest (though still unphysically large) uniform horizontal diffusivity (A_{TH}), we checked and found several second-law violations in our solutions. We repeated run 5 with increased vertical resolution in order to reduce such violations, as recommended by Weaver and Sarachik (1990) and Gerdes et al. (1991). The revised model has 21 levels, spaced in such a way as to almost exactly preserve the 12-level model bottom topography. Second-law violations were greatly reduced in number and severity by the increased resolution. However, the large-scale water mass properties were little changed, implying that the 12-level model solutions are little affected by the resolution-dependent numerical problems.

To test the effect of a smaller horizontal diffusivity on the solution, runs 2 and 4 were repeated with an A_{TH} of 0.4×10^7 cm^2 s^{-1}. In both cases, the solution became significantly contaminated with spurious water masses deriving from pronounced local second-law violations, which were judged to outweigh any potential benefits accruing from the use of the more realistic A_{TH}.

Use of the isopycnal mixing scheme is found to result in greatly diminished convective mixing, especially in runs 4–6. This diminution occurs despite the surface buoyancy forcing being almost unchanged between runs 2–6, and indicates an imperfect implementation of isopycnal mixing. (Ideal isopycnal mixing would be unable to transfer buoyancy upward in place of convective mixing.) For example, a spurious upward buoyancy flux occurs whenever the model's neutral surfaces exceed the maximum allowed mixing slope *and* the neutral surfaces are steepening toward the surface. Such conditions always exist at the base of a convective mixed layer (above which the true neutral surfaces are essentially vertical) leading to buoyancy loss and potential shoaling of the convection. Nevertheless, such spurious transfers have little effect on the overall model solution. The portions of the model ocean subject to convection in run 2 retain extremely weak stratification in runs 3–6, so use of a hypothetical exact isopycnal scheme would result in little density adjustment before the full buoyancy flux were carried by convective mixing.

REFERENCES

Bryan, F., 1987: Parameter sensitivity of primitive equation ocean general circulation models. *J. Phys. Oceanogr.*, **17**, 970–985.

Bryan, K., 1984: Accelerating the convergence to equilibrium of ocean–climate models. *J. Phys. Oceanogr.*, **14**, 666–673.

——, and L. J. Lewis, 1979: A water mass model of the world ocean. *J. Geophys. Res.*, **84**, 347–376.

Bryden, H. L., and T. H. Kinder, 1991: Steady two-layer exchange through the Strait of Gibraltar. *Deep-Sea Res.*, **38**(Suppl.), S445–S463.

Carmack, E. C., 1986: Circulation and mixing in ice covered waters. *The Geophysics of Sea Ice,* N. Untersteiner, Ed., Plenum, 641–712.

Cember R., 1989: Bomb radiocarbon in the Red Sea: A medium scale gas exchange experiment. *J. Geophys. Res.*, **94**, 2111–2123.

Clarke, R. A., 1985: Temporal and spatial scales of Labrador Sea Water formation. North Atlantic Deep Water formation. NASA Conf. Publ. 2367, 7–11.

——, J. H. Swift, J. L. Reid, and K. P. Koltermann, 1990: The formation of Greenland Sea deep water: Double diffusion or deep convection? *Deep-Sea Res.*, **37**, 1385–1424.

Cox, M. D., 1984: A primitive equation, 3-dimensional model of the ocean. GFDL Ocean Group Tech. Rep. No. 1, GFDL/Princeton University, Princeton, N.J., 141 pp.

——, 1987a: Isopycnal diffusion in a z-coordinate ocean model. *Ocean Modelling,* **74**, 1–5.

——, 1987b: GFDL Ocean Model Circular No. 7. GFDL/Princeton University, Princeton, N.J., 1 p.

——, 1987c: GFDL Ocean Model Circular No. 8. GFDL/Princeton University, Princeton, N.J., 2 pp.

——, 1989: An idealized model of the World Ocean. Part I. The global scale water masses. *J. Phys. Oceanogr.*, **19**, 1703–1752.

Cummins, P. F., 1991: The deep water stratification of ocean general circulation models. *Atmos.-Ocean,* **29**, 563–575.

——, G. Holloway, and A. E. Gargett, 1990: Sensitivity of the GFDL ocean model to a parameterization of vertical diffusion. *J. Phys. Oceanogr.*, **20**, 817–830.

England, M. H., 1992: On the formation of Antarctic Intermediate and bottom water in ocean general circulation models. *J. Phys. Oceanogr.*, **22**, 918–926.

——, 1993: Representing the global-scale water masses in ocean general circulation models. *J. Phys. Oceanogr.*, **23**, 1523–1552.

——, J. S. Godfrey, A. C. Hirst, and M. Tomczak, 1993: The mechanism for Antarctic Intermediate Water renewal in a World Ocean model. *J. Phys. Oceanogr.*, **23**, 1553–1560.

Gargett, A. E., 1984: Vertical eddy diffusivity in the ocean interior. *J. Mar. Res.*, **42**, 359–393.

Gent, P. R., and J. C. McWilliams, 1990: Isopycnal mixing in ocean circulation models. *J. Phys. Oceanogr.*, **20,** 150–155.

Gerdes, R., 1993: A primitive equation ocean circulation model using a general vertical coordinate transformation. 2. Application to an overflow problem. *J. Geophys. Res.*, **98,** 14 703–14 726.

——, C. Koberle, and J. Willebrand, 1991: The influence of numerical advection schemes on the results of ocean general circulation models. *Climate Dyn.*, **5,** 211–226.

Godfrey, J. S., 1989: A Sverdrup model of the depth-integrated flow for the World Ocean allowing for island circulations. *Geophys. Astrophys. Fluid Dyn.*, **45,** 89–112.

Gordon, A. L., 1975: An Antarctic oceanographic section along 170°E. *Deep-Sea Res.*, **22,** 357–377.

Grumbone, R. W., 1991: A model of the formation of high salinity shelf water on polar continental shelves. *J. Geophys. Res.*, **96,** 22 049–22 062.

Han, Y-J., 1984: A numerical world ocean general circulation model. Part II. A baroclinic experiment. *Dyn. Atmos. Oceans,* **8,** 141–172.

Hellerman, S., and M. Rosenstein, 1983: Normal monthly wind stress over the World Ocean with error estimates. *J. Phys. Oceanogr.*, **13,** 1093–1104.

Hirst, A. C., and J. S. Godfrey, 1993: The role of Indonesian Throughflow in a global ocean GCM. *J. Phys. Oceanogr.*, **23,** 1057–1086.

Killworth, P. D., 1983: Deep convection in the world ocean. *Rev. Geophys. Space Phys.*, **21,** 1–26.

Kraus, E. B., 1990: Diapycnal mixing. *Climate–Ocean Interaction,* M. E. Schlesinger, Ed., Kluwer, 269–293.

Levitus, S., 1982: *Climatological Atlas of the World Ocean.* NOAA Prof. Paper No. 13., U.S. Govt. Printing Office, Washington D.C., 173 pp.

Lin, C. A., 1988: A mechanistic model of isopycnal diffusion in the ocean. *Climate Dyn.*, **2,** 165–171.

Martin, P. J., 1985: Simulation of the mixed layer at OWS November and Papa with several models. *J. Geophys. Res.*, **90,** 903–916.

McDougall, T. J., 1987a: Neutral surfaces. *J. Phys. Oceanogr.*, **17,** 1950–1964.

——, 1987b: Thermobaricity, cabbeling and water-mass conversion. *J. Geophys. Res.*, **92,** 5448–5464.

Molinari, R. L., E. Johns, and J. F. Festa, 1990: The annual cycle of meridional heat flux in the Atlantic Ocean at 26.5°N. *J. Phys. Oceanogr.*, **20,** 476–482.

——, R. A. Fine, and E. Johns, 1992: The deep western boundary current in the tropical North Atlantic Ocean. *Deep-Sea Res.*, **39,** 1967–1984.

Moore, A. M., and H. B. Gordon, 1994: An investigation of climate drift in a global coupled ocean-atmosphere–sea-ice model. *Climate Dyn.*, in press.

——, and C. J. C. Reason, 1993: The response of a global ocean general circulation model to various climatological surface boundary conditions for temperature and salinity. *J. Phys. Oceanogr.*, **23,** 300–328.

Moum, J. N., and T. R. Osborn, 1986: Mixing in the main thermocline. *J. Phys. Oceanogr.*, **16,** 1250–1259.

Oberhuber, J. M., 1993: Simulation of the Atlantic circulation with a coupled sea ice–mixed layer–isopycnal general circulation model. Part I: Model description. *J. Phys. Oceanogr.*, **23,** 808–829.

Redi, M. H., 1982: Oceanic isopycnal mixing by coordinate rotation. *J. Phys. Oceanogr.*, **12,** 1154–1158.

Rudels, B., D. Quadfasel, H. Friedrich, and M.-N. Houssais, 1989: Greenland Sea convection in the winter of 1987–1988. *J. Geophys. Res.*, **94,** 3223–3227.

Saunders, P. M., 1990: Cold outflow from the Faroe Bank Channel. *J. Phys. Oceanogr.*, **20,** 29–43.

Swift, J. H., 1984: The circulation of the Denmark Strait and Iceland–Scotland overflow waters in the North Atlantic. *Deep-Sea Res.*, **31,** 1339–1355.

——, K. Aagaard, and S.-A. Malmberg, 1980: The contribution of the Denmark Strait Overflow to the deep North Atlantic. *Deep-Sea Res.*, **27A,** 29–42.

Toggweiler, J. R., and B. Samuels, 1993: Is the magnitude of the deep outflow from the Atlantic Ocean actually governed by Southern Hemisphere winds? *The Global Carbon Cycle,* M. Heimann, Ed., Springer-Verlag, 303–331.

——, K. Dixon, and K. Bryan, 1989a: Simulations of radiocarbon in a coarse-resolution World Ocean model. 1. Steady state prebomb distributions. *J. Geophys. Res.*, **94,** 8217–8242.

——, ——, and ——, 1989b: Simulations of radiocarbon in a coarse-resolution World Ocean model. 2. Distributions of bomb-produced Carbon 14. *J. Geophys. Res.*, **94,** 8243–8264.

Weaver, A. J., and E. S. Sarachik, 1990: On the importance of vertical resolution in certain ocean circulation models. *J. Phys. Oceanogr.*, **20,** 600–609.